Competition between surface roughening and reconstruction in (110) facets of fcc crystals

Marcel den Nijs
Department of Physics, FM-15, University of Washington, Seattle, Washington 98195
(Received 6 January 1992)

Surface roughening induces a simultaneous deconstruction transition in missing-row-reconstructed (110) facets of fcc crystals. This transition can be described by the four-state chiral clock-step model. Numerical finite-size-scaling results indicate that at zero chirality this transition has the character of a superimposed Kosterlitz-Thouless-type roughening and an Ising-type deconstruction transition. A symmetry property of the model, called S-T invariance, and related to supersymmetry, elucidates this aspect. In the strong chirality limit a fermion analysis applies. The full phase diagram can be constructed by combining these numerical and analytical results. Pt(110) and Au(110) follow specific paths through it. The only path consistent with the current experimental evidence for Pt(110) is a roughening-induced simultaneous deconstruction transition, which has the character of an incommensurate melting transition with respect to the reconstruction degrees of freedom. This implies that the difference in energy between clockwise and anticlockwise steps is small in Pt(110).

I. INTRODUCTION

The missing-row (MR) -reconstructed (110) facets of face-centered-cubic (fcc) crystals, such as Pt and Au, are among the most extensively studied reconstructed surface structures. Recent progress in experimental techniques and surface preparation make it possible to study the competition between surface roughening and surface reconstruction. This interplay leads to intriguing new types of critical phenomena. For unreconstructed surfaces it gives rise to preroughening (PR) transitions[1-4] and for reconstructed surfaces to the roughening-induced simultaneous deconstruction transition discussed in this paper.[4,5]

The MR nature of the reconstruction in Au(110) was established in the early 1980s, using techniques such as scanning tunneling microscopy.[6] The deconstruction transition was believed to be in the Ising universality class because the MR structure is twofold degenerate. This was confirmed by experimental studies. Campuzano *et al.*[7] found in a low-energy-electron-diffraction (LEED) study of the scaling behavior of the MR diffraction peak that the MR row order parameter vanishes with $\beta=0.13\pm0.02$ ($\beta=\frac{1}{8}$), the correlation length diverges with $\nu=1.02\pm0.02$ ($\nu=1$), and the susceptibility diverges with $\gamma=1.75\pm0.03$ ($\gamma=\frac{5}{4}$). The deconstruction transition in Au(110) was believed to be a prototype experimental realization of an Ising-type phase transition, and attempts were made to test recent theoretical results from conformal field theory.[8] However, at about the same time Villain and Vilfan[9] pointed out that the observed deconstruction temperature $T=0.55T_m$ ($T_m=1336$ K is the melting temperature of Au) is close to the temperature T_R where the (110) facet should roughen. They estimated T_R from approximations of the energy of steps and kinks in those steps. This suggests a competition between surface roughening and surface deconstruction, but they did not address what types of new phase transitions might result because of this. This is the topic of this paper.

The most recent experimental studies still confirm that Au(110) undergoes an Ising-type deconstruction transition, and suggest that the roughening transition is indeed very close; at $T_R\simeq0.59T_m$.[10,11] Recent x-ray experiments for Pt(110) find Ising-type critical exponents as well. Robinson, Vlieg, and Kern[12] observe a deconstruction transition at $T_c=0.53T_m$ with $\beta=0.11\pm0.01$ and $\nu=0.95\pm0.09$ (Pt melts at $T_m=1080$ K). In addition they observe a shift of the liquidlike MR row peak above the deconstruction transition which scales linearly with temperature, $Q\sim|T-T_c|$. The latter can originate only from step excitations, and therefore is a strong indication of competition between roughening and reconstruction. The theoretical results discussed in this paper explain these experimental results.

Last year I proposed that Pt(110) undergoes a roughening-induced simultaneous deconstruction transition, which has the character of a chiral melting transition with respect to its reconstruction degrees of freedom.[4,5] I introduced a model to describe this: the four-state chiral clock-step model. The purpose of this paper is to provide more details of this work and to present more recent results concerning the global structure of the phase diagram of the four-state chiral clock-step model. These results allow me to discuss the nature of the phase transitions along all characteristic paths, and thus to identify which of them is consistent with the experimental results for Pt(110) and Au(110).

The interplay between roughening and reconstruction can be described within the framework of solid-on-solid (SOS) models. The relaxation and buckling of the MR reconstructed surface is sizable. In Au(110) it extends to four layers deep.[13] This certainly has a strong influence on the energies of steps and walls, but these atom displacements are not large enough to invalidate the solid-on-solid description.

The research described in this paper was motivated not only by recent experimental results, but also by my previous work on preroughening phase transitions.[1-4] Koos Rommelse and I discovered the existence of preroughen-

ing (PR) and disordered flat (DOF) phases by a numerical finite-size-scaling study of the restricted solid-on-solid (RSOS) model.[1] The RSOS model applies to (110) facets of simple cubic (sc) crystals. Its phase diagram provides a comprehensive description of surface roughening and reconstruction in such facets, because it includes not only the flat low-temperature phase (at ferromagnetic nearest-neighbor interactions), but also the reconstructed phase (at antiferromagnetic nearest-neighbor interactions). The reconstructed state in this model has a checkerboard-type structure, where all nearest-neighbor columns differ in height by one unit, and all next-nearest-neighbor columns have the same height. I am not aware of any experimental realization of this. Low index facets tend to reconstruct into structures with a much longer period. Fortunately the RSOS model can be modified, without changing the structure of its phase diagram, such that it describes SC (110) facets that reconstruct into the more familiar missing-row (MR) structure. This is described in Sec. II.

The RSOS model displays four types of behaviors.[1–4] A surface which is (ordered) flat at low temperatures can undergo (1) a conventional roughening transition (a path of type 1, using the classification introduced in Ref. 4), or (2) a preroughening transition into a DOF phase followed by a roughening transition at higher temperatures (a path of type 2). When the surface is reconstructed at low temperatures, it can undergo (3) a deconstruction transition followed by a conventional roughening transition at higher temperatures (a path of type 3), or (4) a roughening transition before it deconstructs (a path of type 4).

Experimental evidence for preroughening has surfaced recently in the (111) facets of the rare-gas solids, such as argon and krypton in the form of the so-called "reentrant layer-by-layer growth phenomenon."[14] Moreover, the so-called "onset of anharmonic vibrations" phenomenon in fcc metal surfaces such as Cu(110) and Ni(110) (Ref. 15) can be interpreted as a manifestation of preroughening.[4] There, preroughening can be understood as the result of the competition between the unreconstructed flat and MR reconstructed structures.[3,4] Assume that the MR reconstructed state is close in energy but unfavorable compared to the flat unreconstructed state. At $T>0$, entropy associated with step excitations starts to favor the MR structure, and can stabilize the so-called DOF phase. The DOF phase contains steps that form a disordered structure, but maintain long-range step-up–step-down order.[1,2] The average surface height in the DOF phase is the same as in the MR state, and differs from that in the unreconstructed flat state by one-half unit. Preroughening is the phase transition from the low-temperature unreconstructed flat phase into the DOF phase.[3] The DOF phase is identical to the deconstructed flat phase along paths of type 3, between the Ising-type deconstruction transition and the Kosterlitz-Thouless-(KT) -type roughening transition. The MR structure can be viewed as a close-packed array of steps with alternating step-up–step-down order. The DOF phase is a diluted "step-fluid" version of this where the steps are not close packed anymore and have lost their positional order.

I am not aware of examples of MR reconstructed sc (110) facets. Au(110) and Pt(110) reconstruct in the MR state, but they are fcc crystals. In this paper we will be be preoccupied with the differences between fcc (110) and sc (110) facets. The difference in crystal structure changes the behaviors along paths of type 3 and 4.

Paths of type 1 and 2 are not affected. Phase transitions such as roughening and preroughening are large length scale phenomena. Roughening is described at large length scales by a sine-Gordon model.[16] The appropriate SOS-type model for fcc (110) facets is an anisotropic version of the body-centered solid-on-solid (BCSOS) model, with an interaction range beyond that of the exactly soluble model,[17] but the scaling properties of the roughening and preroughening transition remain the same as in the RSOS model.[18]

The large length scale properties of the preroughening transition are described by this sine-Gordon model as well.[3] At the PR transition the average surface height changes by half a unit. In the sine-Gordon model this means that the amplitude of the leading sine-Gordon operator changes sign. This determines the scaling properties of the PR transition. None of the other differences in the microscopic details matter. Therefore phase diagrams for sc (110) and fcc (110) facets, i.e., the RSOS model and BCSOS model, look alike in the region with paths of type 1 and 2.

In Sec. II we will find that along paths of type 3 and 4, the differences in the underlying crystal structure do matter. In sc (110) facets, described by the RSOS model, the roughening and deconstruction degrees of freedom decouple in the scaling limit. This implies that sc (110) facets can roughen before they deconstruct and implies the existence of an intermediate rough reconstructed phase.[3] In fcc (110) facets, the roughening and reconstruction degrees of freedom couple in an intricate manner. This forces roughening to induce a simultaneous deconstruction transition along paths of type 4.

This observation is the starting point of the research presented here. It leads a study of the scaling properties of this roughening-induced simultaneous deconstruction transition. The BCSOS model with the required increased interaction range is not very suitable for numerical studies. Limited numerical results from Monte Carlo simulations are becoming available only just now.[19] Instead, I introduced a so-called cell-spin model;[4,5] see Sec. 2; a model formulated on a somewhat larger length scale. I called this model the four-state chiral clock-step model, and studied its phase diagram and the scaling properties of its phase transitions by means of the finite-size scaling of its step and wall free energies.[5] These numerical results are presented in detail in Secs. III and VI.

Section IV contains a discussion of S-T invariance. This is a symmetry property of the four-state clock-step model at zero chirality, and related to supersymmetry, which helps to understand why the numerical results of Sec. III indicate that the critical exponents of the roughening-induced simultaneous deconstruction transition are simply Ising-like with respect to the reconstruction degrees of freedom and simply KT-like with respect to the roughening degrees of freedom.

Moreover, the model can be mapped at zero chirality

into a model where an Ising model is coupled to an XY model. This means that the roughening-induced simultaneous deconstruction transition is related to a similar transition in fully frustrated XY models.[20] S-T invariance is a new type of symmetry in that context.

Section V contains a discussion of the phase diagram at strong chirality. In that limit the model reduces to a description for Au (110) proposed recently by Vilfan and Villain.[21] The model is equivalent to a 1D quantum Hubbard model,[22,23] extended with dislocations. I derive the structure of its phase diagram in the continuum limit by bosonization. This type of fermion description of two-dimensional phase transitions is familiar from the theory of commensurate-incommensurate phase transitions in adsorbed monolayers.[24]

In Sec. VI these results are combined into a global structure of the phase diagram, from zero to strong chirality. The characteristic behavior along the various types of paths through the phase diagram is discussed. In Sec. VII we compare this with the current experimental evidence for Au(110) and Pt(110). The results for Pt(110) are consistent only with a path of type 4 at small chirality; i.e., a roughening-induced simultaneous deconstruction transition which is a chiral melting transition into a rough incommensurate (IC) fluid phase with respect to the reconstruction degrees of freedom.

II. STEP AND WALL EXCITATIONS IN MISSING-ROW-RECONSTRUCTED SURFACES

Missing-row (MR) -reconstructed (110) facets of simple cubic (sc) and face-centered-cubic (fcc) crystals behave fundamentally differently, because step and wall excitations in these facets have different topological charges. To demonstrate this fundamental difference, consider first the RSOS model. This is a solid-on-solid model where nearest-neighbor columns of atoms are restricted to differ in height by at most one unit, $dh=0,\pm1$. We discovered preroughening in this model by increasing the interaction range form nearest neighbors (K) to next nearest neighbors (L),[1,2]

$$\mathcal{H}=\sum_{n,m}\{K|h(n,m)-h(n+1,m)|^2 + K|h(n,m)-h(n,m+1)|^2 + L|h(n,m)-h(n+1,m+1)|^2 + L|h(n,m)-h(n-1,m+1)|^2\} . \quad (2.1)$$

At low temperatures with $K<0$ and $L>0$ the surface is reconstructed. It is a checkerboard structure where nearest-neighbor columns differ in height by one step height, $dh=\pm1$, and next-nearest-neighbor columns are equal in height.

This model describes sc (100) facets assuming that the interactions in such surfaces are short ranged and surface distortions, such as buckling and compression in the first few layers, are small. To my knowledge checkerboard-type reconstructions like this have never been observed. Surface reconstructions in low index facets have typically a much longer period.

A simple modification in the interactions makes the RSOS model applicable to (110) facets of sc crystals;

$$\mathcal{H}=\sum_{n,m}\{K_n|h(n,m)-h(n+1,m)|^2 + K_m|h(n,m)-h(n,m+1)|^2 + L|h(n,m)-h(n+2,m)|^2\} . \quad (2.2)$$

This model has a MR-reconstructed phase for $K_n<0$, $L>0$, and $K_m>0$. I do not know of any example of a MR-reconstructed sc (110) facet, but it is instructive to work out the topological aspects of steps and walls in this type of surface, and then to contrast it with those in MR-reconstructed fcc (110) facets (i.e., Pt and Au).

The structure of the phase diagrams of the two models, Eqs. (2.1) and (2.2), is the same, with phase transitions that belong to the same universality class. (Their transfer matrices describe the same spin-1 quantum chain.[2]) The following discussion is valid for both, but it is phrased in the MR language of Eq. (2.2).

Figure 1 shows a side view of the MR state, and of wall and step excitations. The MR state is twofold degenerate and can be represented by an Ising spin variable $S(n,m)=\pm1$, or an angle variable $\theta=\pi n_t$, with $S=\exp(i\theta)$. The two Ising spin states represent the two possible positions of the missing rows, $n_t=1,2$ (mod 2). Define E_w as the wall energy and E_s as the step energy, both per unit length.

The walls and steps are shown in Fig. 1 as idealized "sharp" domain walls. Surface buckling and compression will deform them into less-localized, more soliton-type objects with a width that might extend over several lattice constants. This situation is quite similar to that of domain walls in incommensurate adsorbed monolayers.[24] It is important to realize that the following topological aspects of these excitations are not influenced by the compression or buckling in the top layers, nor by the

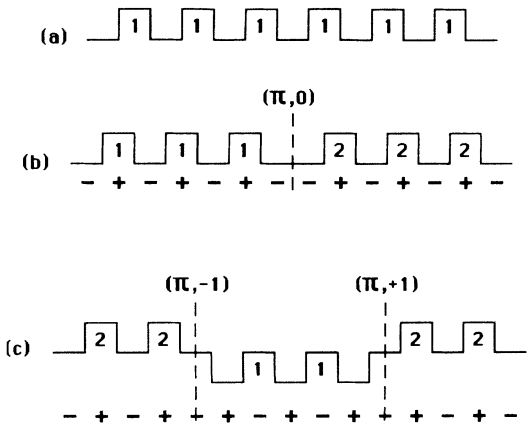

FIG. 1. Side view of (a) a missing-row (MR) -reconstructed simple cubic (110) facet; (b) a wall-type excitation; and (c) a down and up step. The left-right symmetry in (c) illustrates that up and down steps have the same energy. The + and − signs in (b) and (c) illustrate that steps do not affect the MR order.

sharpness of the walls and steps. The topological charges of domain walls are determined by the difference in reconstruction label θ and height h between the domains to the left and right of the domain wall, not by the internal structure of the domain wall. Domain walls cannot change their topological charge, except when they meet. At these domain-wall intersections and dislocations the total topological charge must be conserved.[24]

Wall excitation, see Fig. 1(b), have a topological charge $(d\theta, dh)=(\pi,0)$. Walls do not change the height of the surface, $dh=0$. They couple only to the reconstruction degrees of freedom. Consider a surface where $E_w<E_s$, such that the wall free energy vanishes before the step free energy. This surface follows a path of type 3. First it undergoes an Ising transition into the DOF phase, where the surface remains flat but loses its reconstruction, followed at a higher temperature by a conventional KT-type roughening transition.

Step excitations, see Fig. 1(c), have a topological charge $(d\theta, dh)=(\pi,\pm 1)$. This suggests that steps couple to both types of degrees of freedom. That would imply that along paths of type 4, where steps are more favorable than walls, $E_w>E_s$, the surface roughens and deconstructs simultaneously. This is not true. We can disentangle the order parameters by renaming the Ising spin states, as $\theta\rightarrow\theta+\pi$, each time we cross a step. This is equivalent to an alternative setup, where the reconstruction order is not characterized by the location of the missing rows, but in terms of the parity, $S(n,m)=\exp[i\pi h(n,m)]$. Figure 1(c) illustrates that the antiferromagnetic spin order persists across steps, and therefore that steps do not couple to the reconstruction order. A MR-reconstructed sc (110) facet with $E_w>E_s$ roughens first, via a conventional KT transition, into a reconstructed rough phase, followed at a higher temperature by an Ising-type deconstruction transition, into the deconstructed rough phase. A numerical study of the RSOS model,[1,2] Eq. (2.1), confirms this.

The second definition of the MR order, using parity, is more appropriate also in the context of scattering experiments. The MR diffraction peak persists into the rough reconstructed phase, because columns with the same parity scatter in phase.

It is useful to formulate a cell-spin model. Consider a larger length scale. Imagine a rectangular grid across the surface oriented along the MR grooves. The lattice constants of the grid are large compared to those of the underlying crystal. They must be larger than the widths of the steps and walls (which are comparable to the length scale at which the surface buckles and compresses), and be of the same order of magnitude as the interaction range. The lattice constant must be small compared to the correlation length, and also to the density of steps and walls. These conditions are satisfied close to the roughening and deconstruction transition in surfaces where these transitions are close in temperature such that the correlation length remains large.

Associated with each cell of the grid is an Ising spin, $S_r=\exp(i\theta_r)$, to represent the reconstruction inside the cell, and a height variable h_r to represent the surface height. The simplest cell spin Hamiltonian has the form

$$\mathcal{H}=-\sum_{\langle r,r'\rangle}\{\tfrac{1}{2}K_s S_r S_{r'} + (\tfrac{1}{2}K_t S_r S_{r'}+Q)[1-2(h_r-h_{r'})^2]\} . \quad (2.3)$$

We can assume that the height variables obey the RSOS restriction, $dh=h_r-h_{r'}=0,\pm 1$, because steps with a step size larger than 1 are expensive, and $|dh|>1$ height differences between nearest-neighbor cells are unlikely when the step density is small compared to the size of the cells. Kinks in the steps and walls have their own energy. Therefore the coupling constants in the horizontal and vertical direction should be different. This can be taken care of partially by keeping the coupling constants isotropic, while choosing the cell-spin lattice, the grid, to be anisotropic. Equation (2.3) does not include interactions between steps and walls at nearby bonds of the grid, nor does it include core energies associated with the merging and crossing of walls at vertices of the grid. This could be taken care of by extending the interaction range. None of these fine tunings of the model will change the scaling properties of the phase transitions.

In the cell-spin model, Eq. (2.3), the energy of a wall, $(d\theta, dh)=(\pi,0)$, is equal to $E_w=K_s+K_t$. The energy of a step $(d\theta, dh)=(0,\pm 1)$ is equal to $E_s=K_t+2Q$. In addition, the cell-spin model allows steps of type $(d\theta, dh)=(\theta,\pm 1)$. These have an energy $E_{s'}=K_s+2Q$. In the microscopic model, Eq. (2.2), these steps are forbidden. In the cell-spin model they are allowed, because they represent excitations with a wall and a step inside the same cell. $-2K_t$ is the repulsion energy between such a wall and step, $E_{s'}=E_w+E_s-2K_t$, and can be expected to be negative, $K_t/K_s<0$.

We can interchange the roles of the two-step-type excitations in the cell-spin model. Suppose we do not choose the Ising variable in the RSOS model in terms of the parity, $S=\exp(i\pi h)$, but in terms of the location of the missing rows in the MR reconstruction, as we did initially in the discussion above. Now the $(d\theta, dh)=(0,\pm 1)$ steps are forbidden in the microscopic model, and they are the ones that represent a bound state of one wall and one step. In this formulation K_s must be negative, $K_s/K_t<0$, because $K_s=E_w+E_{s'}-2K_s$. This transformation interchanges the roles of K_s and K_t. We will discuss this symmetry in more detail in Sec. IV.

fcc (110) facets have an anisotropic body-centered-type structure. Atoms in adjacent layers are not located on top of each other, but on top of the plaquettes; see Fig. 2. This difference leads to fundamentally different topological charges of walls and steps. Figure 3(a) shows a side view of the MR state in fcc (110) facets. In this schematic representation adsorbing a particle corresponds to adding a brick, one unit wide and two units high. The MR structure in fcc (110) facets is characterized by an angle variable $\theta=\frac{1}{2}\pi n_t$, representing the four possible positions of the missing rows, $n_t=1,2,3,4$ (mod 4). The MR state is only twofold degenerate, because for each specific surface height only $\theta=0,\pi$ or only $\theta=\pm\frac{1}{2}\pi$ can be realized. These two sets alternate with each change in height by one unit.

Again we can distinguish between walls and steps, see

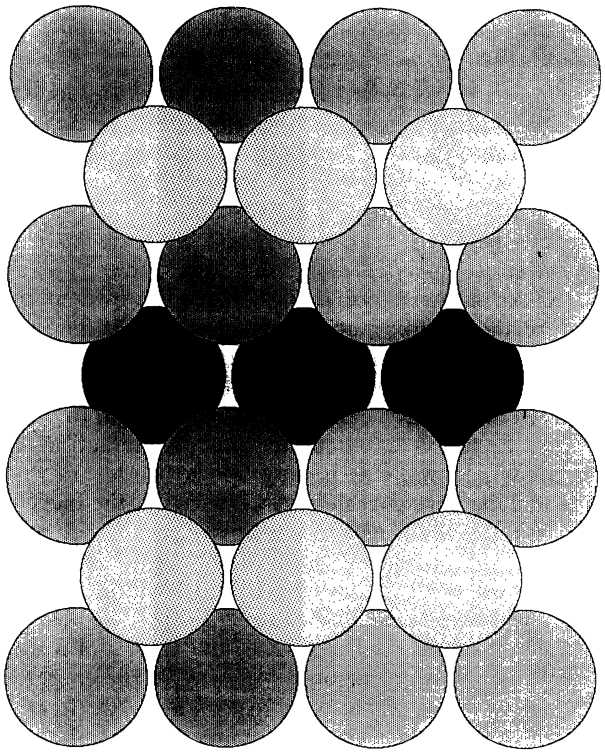

FIG. 2. Top view of a missing-row-reconstructed fcc (110) facet.

Figs. 3(b)–3(d), and identify their topological charge $(d\theta, dh)$. The walls and steps in Fig. 3 are again only a guide to the eye. They are shown as sharp objects that would apply if the surface did not compress nor buckle in its top layers. The width of the walls and steps in Pt(110) and Au(110) is yet unknown, but they must look more diffuse than shown in Fig. 3, because these surfaces show a sizable compression and buckling (with the MR periodicity) up to the fourth layer. This has been observed experimentally,[13] and also has been found theoretically in zero-temperature energy calculations.[25]

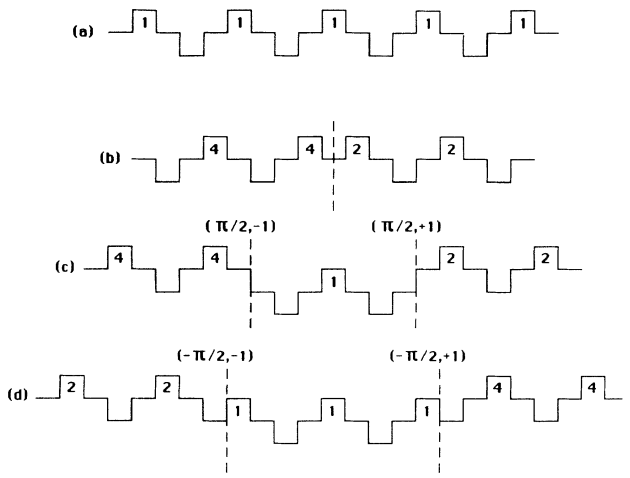

FIG. 3. Schematic side view of (a) a missing-row-reconstructed fcc (110) facet; (b) a wall-type excitation; (c) a clockwise down and up step; and (d) an anticlockwise down and up step. The left-right symmetry in (c) and (d) illustrates that step energies of up and down steps are the same.

It would be very helpful if those theoretical calculations could be extended to calculate the properties of walls and steps. We need to know the internal structure of domain walls (in particular their width). The model defined below needs as input parameters the values of domain-wall energies, their interaction energies, their kink energies, and core energies associated with domain-wall crossings and dislocations. At this time we lack sufficient insight in these aspects. Therefore I leave them as free parameters. In Sec. VI, after obtaining the full phase diagram, we will address this issue again.

At every $(d\theta = \pm\frac{1}{2}\pi)$-type domain wall the height change is odd (these are the steps). At every $(d\theta = \pi)$-type domain wall the height change is even (these include the walls, which by definition have $dh = 0$). Figures 3(b)–3(d) show all the topological distinct domain walls, with step heights smaller than or equal to 1. There are two types of steps, clockwise (C) and anticlockwise (AC) steps. The reconstruction variable θ rotates clockwise or anticlockwise when crossing the step from left to right along vertical bonds of the grid. The internal structure of clockwise steps, and also of AC steps, is the same whether the step is up or down. This is illustrated in Figs. 3(c) and 3(d) by the left-right symmetry. So the step energies depend only on $d\theta$.

Important aspects, such as the observed shift in the MR diffraction peak in Pt(110),[12] are determined by the topological charge of the steps, not by how sharp or internally relaxed they are. The peak shift reflects a temperature-dependent average rotation of θ across the surface with an incommensurate period. The MR unit cell translates laterally across each clockwise (anticlockwise) step forward (backward) over $d\theta = \frac{1}{2}\pi$ $(d\theta = -\frac{1}{2}\pi)$. The peak shift implies that the density of clockwise and anticlockwise steps is different. Indeed, C and AC steps have a different energy due to the difference in their microscopic internal structure. The direction in which the MR peak shifts in Pt(110) (Ref. 12) indicates that the clockwise steps are energetically favorable.

The steps in MR-reconstructed (110) fcc crystals couple to both the reconstruction and roughening degrees of freedom, $(d\theta, dh) = (\pm\frac{1}{2}\pi, \pm 1)$. The same seemed to be true for sc (110) facets in the same type of setup where the reconstruction order parameter is defined by the location of the missing rows. But for the sc (110) facets we found that the steps decouple from reconstruction in the parity definition of the reconstruction order parameter, $S = \exp(i\pi h)$. Surface roughening and reconstruction decouple for sc (110) facets. Such a transformation does not exist for fcc (110) facets. It is impossible to redefine and link the θ variables with the surface height, in such a way that both the C and AC steps do not couple to the reconstruction degrees of freedom anymore. For example, consider redefining the reconstruction variable as $\theta \rightarrow \theta - h \bmod(4)$. This sets $d\theta = 0$ at C and AC up steps but leaves a $d\theta = \pi$ at C and AC down steps. So surface roughening and reconstruction are intricately coupled. Roughening and deconstruction must take place simul-

taneously in fcc (110) facets where steps are energetically more favorable than walls.

To determine the scaling properties of this roughening-induced simultaneous deconstruction transition we need to formulate a model. One appropriate model is an extended version of the BCSOS model. In this model nearest-neighbor columns must differ by $dh=\pm 1$. The BCSOS model is exactly soluble with next-nearest-neighbor coupling only.[17] To induce a MR-reconstructed state requires an increase in the range of the interactions, at least up to third neighbors. This makes the BCSOS model less attractive for numerical calculations. Limited numerical results for this model are becoming available only now.[19]

A more effective way to study the scaling properties of this phase transition is to define a cell-spin model, like the one above for the sc facets. Imagine a rectangular grid oriented along the grooves of the missing rows just like before in the sc facets. Each cell is large compared to the MR unit cell, but small compared to the correlation length. Associate with each cell a $\theta_{n,m}=0,\pm\frac{1}{2}\pi,\pi$ clock variable to represent the four MR states. The simplest cell-spin Hamiltonian has the form

$$Z=\sum_{\{\theta_{n,m}\}}\exp\left\{\sum_{n,m}[K_m\cos(\theta_{n,m}-\theta_{n,m+1}-\Delta)+Q_m\cos(2\theta_{n,m}-2\theta_{n,m+1})+K_n\cos(\theta_{n,m}-\theta_{n+1,m})\right.$$
$$\left.+Q_n\cos(2\theta_{n,m}-2\theta_{n+1,m})]\right\}Z_{6V}(\{d\theta=\pm\tfrac{1}{2}\pi\},L)\ . \tag{2.4}$$

This is a four-state clock model with chiral symmetry breaking, and with every configuration weighted by a six-vertex (6V) model. The θ variables describe the positions of steps and walls and the reconstruction aspect $d\theta$ of their topological charge. The 6V part of the Hamiltonian describes the step height aspect dh of the steps. In the conventional 6V model arrows are placed on all the bonds of a rigid lattice. The 6V model in Eq. (2.4) is defined on an annealed fluctuating lattice, the one formed by the $d\theta=\pm\frac{1}{2}\pi$ steps of the clock model. Walls, the $d\theta=\pi$ excitations of the clock model, are excluded because they do not change the surface height. At each vertex of this lattice formed by the steps the flux of arrows must be zero. The 6V arrows represent the change in height at the steps. The height of the terrace to the left of the step is one unit lower than the terrace to the right when you orient yourself in the direction pointing along the arrow. See Refs. 1 and 2 for a similar formulation of the RSOS model as an Ising model coupled to a 6V model.

Equation (2.4) is a hybrid formulation, a combination of a spin model and a vertex model. This is by necessity. It is incorrect to simply associate to each cell a height variable h_r and a clock variable θ_r and to introduce the simplest Hamiltonian where a four-state clock and SOS model couple to each other. We did this in Eq. (2.3) for the sc facets and found that it introduced new types of domain walls, the $(\pi,1)$ domain walls, which are energetically unlikely, but are allowed by the topology and will be generated under renormalization (a wall and step inside the same cell). For fcc facets this procedure would introduce domain walls with topological charges such as $(d\theta,dh)=(\pi,1)$, which are strictly forbidden, and cannot be generated under renormalization.

In Sec. IV we will discuss a simpler formulation of Eq. (2.4), valid at zero chirality, $\Delta=0$; Eq. (2.4) can be rewritten in the form of Eq. (2.3) with $K_t=K_s$. A different alternative is to represent the chiral four-state clock-step model as a vertex model. Each bond of the lattice can be in six possible states: empty, a clockwise up or down step, an anticlockwise up or down step, or a wall. These six states can be presented by solid and dashed lines with arrows (the steps) and dots (the walls). The only allowed configurations are those where at each vertex the flux of arrows is zero and also the total change in θ is zero mod 2π. There are 152 such vertex states. This formulation is most convenient for numerical FSS calculations, and will be used in Secs. III and VI.

K_m, Q_m, and Δ in Eq. (2.4) represent the energies of the steps and walls:

$$E_{cs}=K_m[\cos(\Delta)-\sin(\Delta)]-2Q_m\ ,$$
$$E_{as}=K_m[\cos(\Delta)+\sin(\Delta)]-2Q_m\ , \tag{2.5}$$
$$E_w=2K_m\cos(\Delta)\ .$$

These energies depend only on the clock variable, because the microscopic structure of steps is independent of whether the step is up or down, $dh=\pm 1$ [the left-right symmetry in Figs. 3(c) and 3(d)]. Clockwise steps, $d\theta=\frac{1}{2}\pi$, and anticlockwise steps, $d\theta=-\frac{1}{2}\pi$, have a different microscopic structure and therefore a different energy. This is called chirality, and is represented by Δ. K_n and Q_n represent the energy of kinks in the steps and walls. Steps and walls repel or attract each other at short distances. L represents a repulsion between up-up (down-down) steps. Other domain-wall interactions are missing in Eq (2.4). Core energies of domain-wall intersections and dislocations are missing too. It is possible to include all these aspects, but I believe that Eq. (2.4) contains all interactions essential to study the nature of the phase transition.

Chiral clock models without these novel height degrees of freedom are familiar from the theory of commensurate-incommensurate transitions in adsorbed monolayers.[24] The analysis in the following sections is guided by experience from those models where our understanding of the phase diagram is based on detailed knowledge of two limit cases, namely zero and strong chirality.

III. NUMERICAL RESULTS AT ZERO CHIRALITY

This section contains the results of a numerical finite-size-scaling study of the phase diagram of the four-state chiral clock-step model, Eq. (2.4), at zero chirality, $\Delta=0$. In this limit clockwise and anticlockwise steps have the same energy. The purpose is to obtain the scaling properties of the roughening-induced simultaneous deconstruction transition. Without loss of generality we will choose isotropic interactions $K_n=K_m$ and $Q_n=Q_m$, see Eq. (2.4), and turn off the step-step interaction, $L=0$.

Figure 4 shows the phase diagram obtained from the numerical study discussed below. $R=E_w/E_s$ is the ratio between the step and wall energy. Temperature T is measured in units of the step energy E_s. At small R, where walls are more favorable than steps, the surface deconstructs first into a disordered flat (DOF) phase, and roughens only at a higher temperature. This represents paths of type 3 in the classification of Sec. I. At $R=2.0\pm0.1$ the roughening and deconstruction lines meet and merge for $R>2$ into a single roughening-induced simultaneous deconstruction transition. This represents crossover to paths of type 4.

I study the finite-size-scaling (FSS) behavior of interface free energies in semi-infinite strips. The method is the same as in earlier studies of, for example, preroughening in the RSOS model.[1,2] In the RSOS model each vertical bond can be in only $q=3$ possible states (an up or down step, or no step), but in the four-state clock-step model q is much bigger, $q=6$ (a clockwise or anticlockwise up or down step, a wall, or no domain wall). The calculation requires that a state vector of size q^N be stored. This scales exponentially with strip size. The maximum accessible strip width is therefore quite small, $N_m=7$ for the computer I used. Due to this limitation the results are not as conclusive compared to those in, e.g., the earlier study of the RSOS model. Additional numerical work will be needed to confirm some of the results in more detail. One of the purposes of the following rather detailed account of my numerical results is to provide a reference frame for such future work. One of the possible alternative methods is a Monte Carlo FSS study, similar to those applied to the conventional chiral clock models.[24,26]

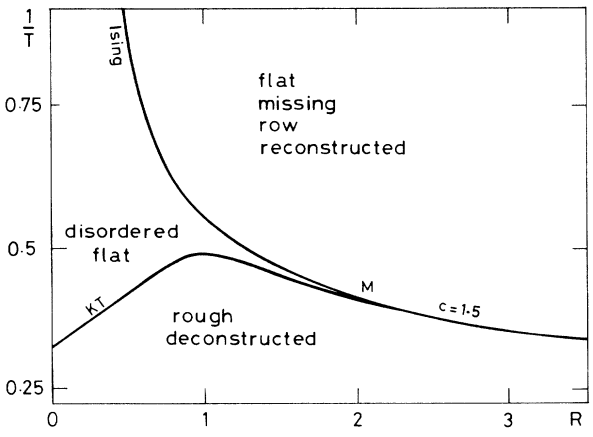

FIG. 4. Phase diagram of the four-state clock-step model at zero chirality ($\Delta=0$), with $R=E_w/E_s$ the ratio of the wall and step energy, and temperature T in units of the step energy E_s.

The phase diagram and the scaling properties of phase transitions follow from the FSS behavior of interface free energies. Consider semi-infinite lattices with different types of boundary conditions in the finite lattice direction: $\theta(n+N,m)=\theta(n,m)+\phi$ and $h(n+N,m)=h(n,m)+k$. The topological charges of the step and wall excitations in the model restrict the possible boundary conditions as $(\phi,k)=(0,2n)$, $(\pi,2n)$, and $(\pm\frac{1}{2}\pi,2n+1)$, with n an integer. The free energy for each of these boundary conditions is related to the largest eigenvalue λ_0 of the transfer matrix as $f(\phi,k)=-N\ln(\lambda_0)$. Define $\eta(\phi,k)$ as the difference in free energy with respect to periodic boundary conditions, $\eta(\phi,k)=N[f(\phi,k)-f(0,0)]$. Each boundary condition forces a specific wall, step, or a combination of steps and/or walls into the surface. Which of these is realized depends on the ratio between the step energy and the wall energy, $R=E_s/E_w$.

Consider, for example, the $(\phi,k)=(\pi,0)$ boundary condition. In the limit $R\ll2$, where steps are frozen out, it forces a wall excitation, Fig. 3(b), into the surface across the entire lattice in the infinite lattice direction. So $\eta(\pi,0)$ represents the free energy of a wall. In the opposite limit, $R\gg2$, where walls are frozen out, the boundary condition forces two clockwise steps with opposite dh, Fig. 3(c), or two anticlockwise steps with opposite dh, Fig. 3(d), into the surface. In this limit, $\eta(\pi,0)$ represents the free energy of two steps. The character of $\eta(\pi,0)$ changes at the wetting line. This is the line inside the ordered low-temperature phase where $\eta(\pi,0)$ becomes equal to two times $\eta(\pm\frac{1}{2}\pi,\pm1)$. The wetting line starts at zero temperature at $R=2$, and ends at the multicritical point M, at $R\simeq2$; see Fig. 4. (I did not verify this numerically.) At the $R<2$ side of the wetting line the boundary condition forces a wall into the surface. But towards the wetting line, for increasing R and increasing T the wall changes in character from a sharp object, as in Fig. 3(b), into a composite broadened object, composed of a bound pair of two clockwise or two anticlockwise steps with opposite dh, as in Figs. 3(c) and 3(d). At the wetting line this bound pair (the composite wall) unbinds into two independent step excitations.

The structure of the phase diagram and the scaling properties of the phase transitions follow from the FSS scaling behavior of these $\eta(\phi,k)$'s. They vanish at different phase transitions. For example, $\eta(\pi,0)$ is conjugate to the missing-row (MR) order parameter. Its vanishing indicates the disappearance of the MR reconstruction order. $\eta(\pi,0)$ is zero in the rough deconstructed phase, and also in the DOF phase. $\eta(\pi,0)$ is nonzero in the flat reconstructed phase and would also be nonzero in the rough reconstructed phase. The latter phase is absent according to the arguments in Sec. II, but we want to confirm this numerically.

$\eta(0,2)$ represents the free energy of a clockwise-anticlockwise step pair, both with $dh=1$. It couples only to the surface roughness. $\eta(0,2)$ is zero in the rough deconstructed phase and finite in both flat phases (the

MR-reconstructed phase and the DOF phase). $\eta(0,2)$ would be zero in the rough deconstructed phase.

$\eta(\pi,1)$ represents the free energy of a single step excitation. It couples simultaneously to the MR and the roughening degrees of freedom. Therefore, it is zero only in the rough deconstructed phase.

Consider the deconstruction transition. $\eta(\pi,0)$ must be finite at the low-temperature side, be zero at the high-temperature side, and scale as a power law at T_c. Figure 5 shows the lines where the $N\eta(\pi,0)$ curves at successive values of N cross, $N\eta(\pi,0)_N=(N-1)\eta(\pi,0)_{N-1}$, for $N=4-7$. These so-called crossing points must converge to the deconstruction critical line in the limit $N\to\infty$.

The deconstruction transition at $R<2$ must be in the Ising universality class. At an Ising transition $\eta(\pi,0)$ must scale as $N\eta(\pi,0)=2\pi x_H$; with a universal amplitude $2\pi x_H=2\pi\beta/\nu=\frac{1}{4}\pi$. This provides an alternative method to determine the location of the deconstruction critical line. Figure 6 shows the lines where $N\eta(\pi,0)_N=\frac{1}{4}\pi$ for $N=3-7$. These lines converge to the same estimate of T_c as the ones in Fig. 5. It does this not only at $R<2$ but also along the roughening-induced deconstruction line at $R>2$.

The vanishing of the interface free energies $\eta(\frac{1}{2}\pi,1)$ and $\eta(0,2)$ indicate surface roughening. In the rough phase they scale as power laws: $\eta(\frac{1}{2}\pi,1)=\frac{1}{2}K_G/N$ and $\eta(0,2)=2K_G/N$, with K_G the roughness parameter. K_G decreases continuously with temperature. The location of the roughening transition line follows from the condition that at a KT transition the roughness parameter must take the universal value $K_G=\frac{1}{2}\pi$, i.e., that $N\eta(0,2)=\pi$. Figure 7 shows the lines where $N\eta(0,2)_N=\pi$.

At $R<2$, surface roughening takes place at a higher temperature than surface deconstruction. Figures 5–7 show that at $R\simeq 2$ the roughening and deconstruction lines meet. As predicted in Sec. II they do not cross. At $R>2$ the FSS estimates of the roughening transition in Fig. 7, and the MR deconstruction transition in Figs. 5 and 6, converge as function of N to the same temperature. The reconstructed rough phase does not exist.

The step free energy $\eta(\frac{1}{2}\pi,1)$ is special, because it couples simultaneously to the MR and roughening degrees of freedom. Figure 8 shows the crossing points of this quantity, i.e., the lines where $N\eta(\frac{1}{2}\pi,1)_N=(N-1)\eta(\frac{1}{2}\pi,1)_{N-1}$. I did not expect this to be a good indicator of the transition lines, because $\eta(\frac{1}{2}\pi,1)$ should scale as a power law not only at T_c but also everywhere

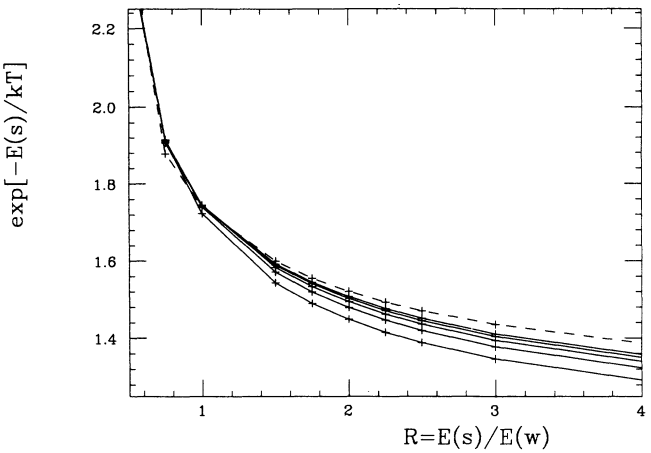

FIG. 6. Finite-size-scaling estimates for the location of surface deconstruction by requiring that the universal amplitude of $\eta(\pi,0)$ takes the universal value $\frac{1}{4}\pi$. The solid lines show where $N\eta(\pi,0)_N=\frac{1}{4}\pi$ at successive values $N=3$, 4, 5, 6, and 7. These lines converge smoothly towards the dashed line, which represents a power-law extrapolation.

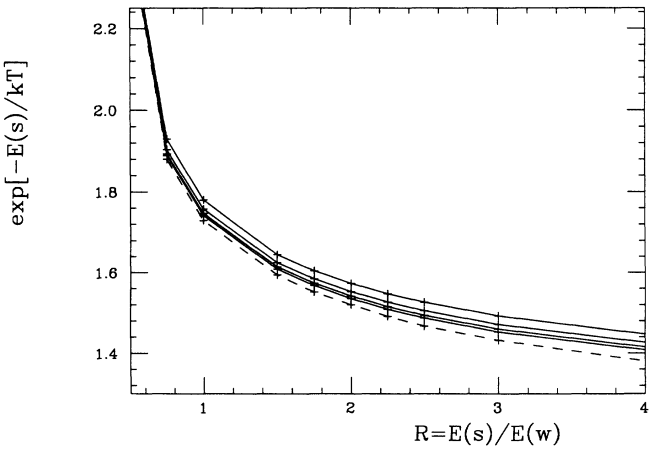

FIG. 5. Finite-size-scaling estimates for the location of surface deconstruction from the crossing points of $\eta(\pi,0)$. The solid lines show the crossing points at successive values $(N,N+1)=(3,4)$, (4,5), (5,6), and (6.7). These lines converge smoothly towards the dashed line, which represents a power-law extrapolation.

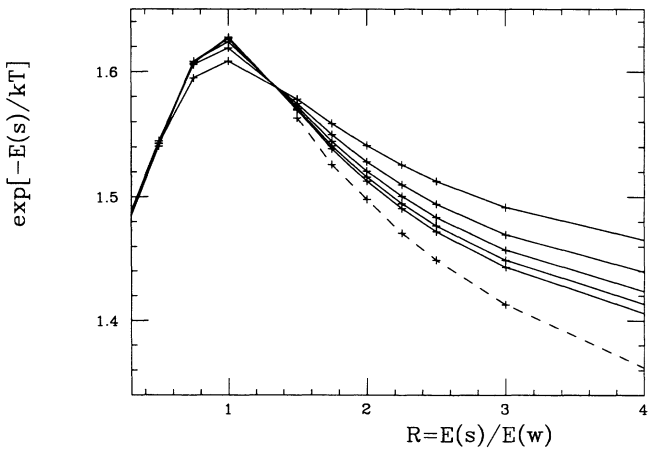

FIG. 7. Finite-size-scaling estimates for the location of surface roughening by requiring that the universal amplitude of $\eta(0,2)$ takes the universal value π. The solid lines show where $N\eta(2,0)_N=\pi$ at successive values $N=3$, 4, 5, 6, and 7. These lines converge smoothly towards the dashed line, which represents a power-law extrapolation.

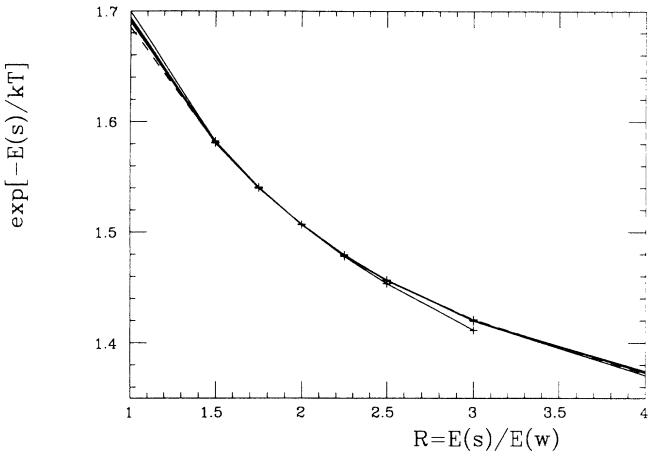

FIG. 8. Finite-size-scaling estimates for the location of surface roughening from the crossing points of $\eta(\frac{1}{2}\pi,1)$. The solid lines show the crossing points at successive values $(N,N+1)=(3,4)$, (4,5), (5,6), and (6,7). Corrections to scaling in this quantity are small.

inside the rough phase. At $R>2$ these crossing points lead to the same estimate of the roughening-induced deconstruction line as the previous quantities. Actually, it seems to be a much better indicator, because corrections to scaling in this quantity are virtually absent. The reason for this is yet unclear; often this indicates the presence of an exact duality-type symmetry in the model.

Figure 9 gives a resume of the different conditions used to determine the structure of the phase diagram. It shows the dashed lines from Figs. 5–8. These follow from power-law extrapolations, $W(N)=W_c+AN^{-x}$, with $W=\exp[-E(s)/k_BT]$, to the data at finite N. I compared extrapolations with free and various fixed values of the leading correction to scaling exponent x.

The success of FSS studies like this resides in the fact that the η's are known to arbitrary high precision at a sequence of strip widths, $N<N_m$, and that their finite-size-scaling behavior is smooth and often dominated by one or only a few corrections to scaling exponents at already relatively small values of N_m. For example, the leading corrections to the scaling exponent x have been determined accurately for several models.[27] However, in the present case the upper limit to the strip width is so small, $N_m=7$, that I feared that the asymptotic scaling region would not be reached sufficiently to draw reliable conclusions about the structure of the phase diagram and the critical exponents. Fortunately the corrections to scaling behave quite smoothly. Moreover, I checked the FSS behavior of a rather large set of quantities and detected no anomalies. All numerical results support each other.

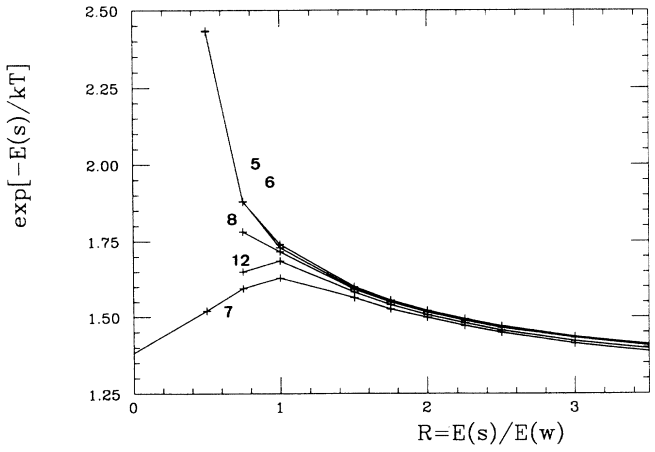

FIG. 9. Resume of the various estimates for the location of surface roughening and deconstruction. The shown curves are the dashed lines (the extrapolations) from Figs. 5–8 and 12, and are numbered accordingly.

The above results confirm the existence of the roughening-induced simultaneous deconstruction transition; the roughening and Ising deconstruction line merge at $R=2.0\pm0.1$. Originally I expected the transition at $R>2$ to be first order. But there is no evidence for that. The deconstruction and roughening critical lines merge smoothly, and we will see next that the critical exponents do not seem to change.

The curves in Fig. 7 represent finite-size estimates of the line where the roughness parameter is equal to the universal value it must take at a KT-type roughening transition, $K_G=\frac{1}{2}\pi$. K_G should not be able to reach this value if the transition is first order. The KT instability would be preempted by a different mechanism. The $K_G=\frac{1}{2}\pi$ condition should still extrapolate to the correct transition temperature, because at the transition K_G jumps to ∞, but each estimate at finite N should underestimate the roughening temperature. The lines in Fig. 7 indeed underestimate T_c, but not in a very significant manner. The effect is of the same order of magnitude as the FSS corrections in the deconstruction-type finite-size estimates in Figs. 5 and 6. Moreover this type of convergence from the low-temperature side of T_c is common in numerical studies of KT transitions as well.[28] More significant is that the FSS estimates in Fig. 7 do not cross with those in Figs. 5 and 6, and nowhere to the right of the multicritical point M. I would have considered a crossing to be an indication of a possible first-order transition.

Compare Figs. 5 and 6. The crossing points in Fig. 5, and the condition $N\eta(\pi,0)=\frac{1}{4}\pi$ in Fig. 6, must agree about the location of the transition line, irrespective of whether the transition is first or second order. In both cases $\eta(\pi,0)$ jumps from its finite value at the low-temperature side to zero at the high-temperature side, and the crossing points must converge to this point. We already checked this, but now we need to focus on the values of $N\eta(\pi,0)$ at the crossing point.

If the transition is second order, the value of $N\eta(\pi,0)$ at the crossing point must converge to the universal FSS amplitude $N\eta(\pi,0)=2\pi x_H$, with x_H the order-parameter critical exponents characteristic of this second-order transition. If the transition is first order, $\eta(\pi,0)$ is not likely to scale as a power law. Figure 10 shows the values of $N\eta(\pi,0)$ at the crossing points. They converge well, indicating a second-order transition at $R>2$. At very

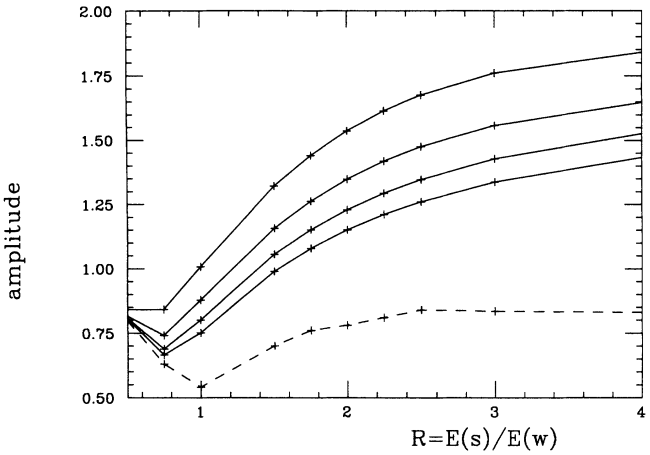

FIG. 10. Finite-size-scaling estimates for the universal amplitude A of the interface free energy $\eta(\pi,0)\simeq A/N$. The solid lines show the value of $N\eta(\pi,0)$ at the crossing points shown in Fig. 5, at successive values $(N,N+1)=(3,4)$, (4,5), (5,6), and (6.7). The convergence is smooth towards the dashed line, which represents a power-law extrapolation.

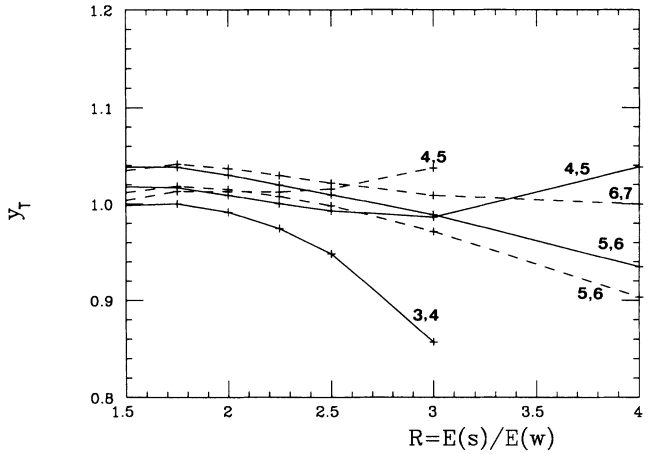

FIG. 11. Finite-size-scaling estimates for the thermal critical exponent y_T along the roughening-induced simultaneous deconstruction line from the scaling behavior of the first temperature derivative, $d\eta(\frac{1}{2}\pi,1)/dT$, at the crossing points of $\eta(\frac{1}{2}\pi,1)$ shown in Fig. 8. From each pair of crossing points, at $(N,N+1)$ and $(N+1,N+2)$, two estimates for y_T are constructed; one from the two lower sizes, N and $N+1$ (the solid lines), and one from the two upper sizes $N+1$ and $N+2$ (the dashed lines).

small values of R where the model reduces to the Ising model, the amplitude converges rapidly to the correct Ising value. At intermediate values, $0.75<R<2$, where the DOF phase becomes very narrow, the convergence is bad, likely due to the corrections to scaling from the multicritical point M. Along the roughening-induced reconstruction line, at $R>2$, the convergence improves again. The dashed line shows the extrapolated values using a power-law fit $N\eta(\pi,0)_N=N\eta(\pi,0)+AN^{-x}$ with x the leading correction to scaling exponent; x is of order $x\simeq 1.0$ for $R\geq 2$. The universal amplitude is equal to $N\eta(\pi,0)=0.81\pm 0.03$, consistent with the value at an Ising transition. This is a surprise. It suggests that the roughening-induced deconstruction transition has Ising-type critical exponents.

The specific-heat critical exponent $\alpha=(2y_T-2)/y_T$ can be determined from the FSS behavior of the temperature derivatives of the η's. At T_c these derivatives should scale as $d(N\eta)/(dT)\simeq AN^{y_T}$. I checked this for all three η's at the crossing-point lines and also all other criteria used above to determine T_c. Estimates for the amplitude A and exponent y_T are constructed from the values of $d(N\eta)/(dT)$ at consecutive values of N. The results converge reasonably. They are not very accurate, because $N_m=7$, but for every η it leads to a $y_T=1.0\pm 0.1$ along the entire critical line (for $2<R<4$). Figure 11 shows the results for $\eta(\frac{1}{2}\pi,1)$, which are better than those for the other two η's, because of the virtual absence of corrections to scaling in this quantity. It is likely that logarithmic factors are present in the FSS behavior of these temperature derivatives. The coupling between the Ising and roughening degrees of freedom might generate such terms because the roughening sector contains marginal operators. At the available system sizes, $N_m=7$, the above simple power-law fit seems adequate, however.

Another interesting quantity that informs us about the nature of phase transitions is the central charge c. This parameter characterizes the universality class of two-dimensional phase transitions from the perspective of conformal field theory.[29] For example, at Ising-type transitions $c=0.5$, and inside a rough phase $c=1.0$. The central charge can be obtained from the universal FSS amplitude of the singular part of the free energy with periodic boundary conditions,[29]

$$f(0,0)_N=f_{\rm reg}-\tfrac{1}{6}\pi cN^{-2}\ . \tag{3.1}$$

Each pair of strip sizes, N and $N+1$, yield a FSS estimate for c, $c(N,R,T)$, at each temperature, which at T_c should converge to the value of c characteristic for the phase transition under consideration, and converge to zero away from criticality.

Inside the rough phase the $c(N,R,T)$ converge to the correct value $c=1$, and at low T converge to zero as expected. For $R>1$ each $c(N,R,T)$ at fixed N has a maximum as function of T. $c(N,R,T)$ swings up and shows a maximum. This is in accordance with the so-called c theorem,[30] and its gives us yet another way to estimate the location roughening-induced deconstruction line. The c theorem implies that higher-order critical points in the phase diagram must have a larger value of c. So at the roughening-induced deconstruction transition c must be larger than its value inside the rough phase, $c=1.0$, and the $c(N,R,T)$ should indeed have a maximum.

These lines of maxima, $c_m(N,R)$, are shown in Fig. 12. As expected, they scale with N to the same estimate of the roughening-induced deconstruction line as our earlier criteria. The dashed line in Fig. 12 is included in Fig. 9. The value of c at these maxima, see Fig. 13, converges to $c=1.50\pm 0.05$ for all $R>2$. This value of c is surprising. It suggests that Ising ($c=0.5$) and KT roughening ($c=1.0$) critical behavior are simply superimposed. Also

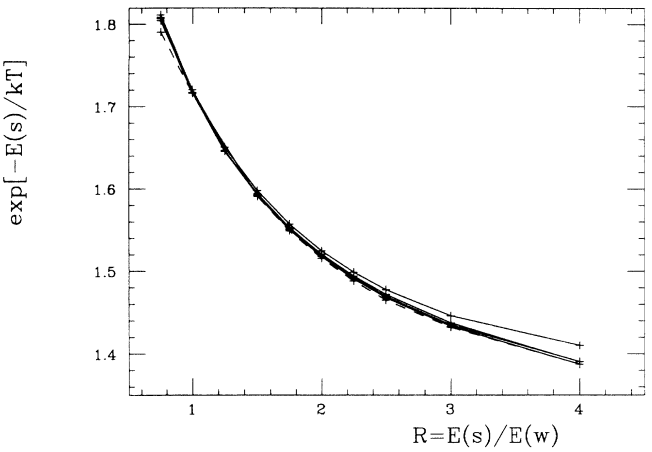

FIG. 12. Finite-size-scaling estimates for the location of the roughening-induced simultaneous deconstruction line from the central charge. The solid lines show the temperatures at which the estimate $c(N,R,T)$, defined in the text, has a maximum with respect to temperature at successive values $(N,N+1)=(3,4)$, (4,5), (5,6), and (6,7). The corrections to scaling are small. The dashed line represents a power-law extrapolation.

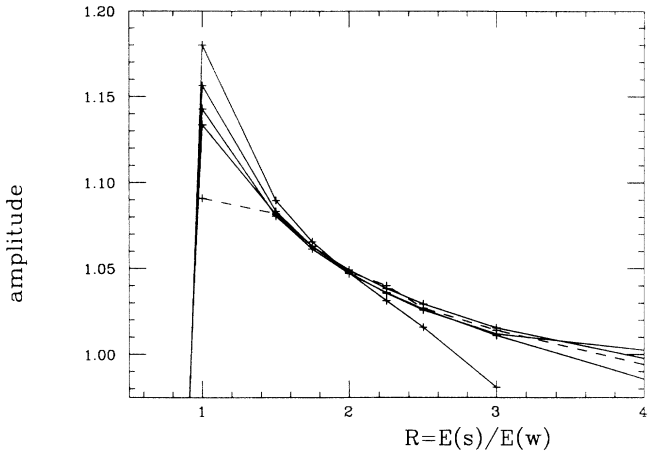

FIG. 14. Finite-size-scaling estimates for the universal amplitude A of $\eta(1,1)\simeq A/N$ along the roughening-induced simultaneous deconstruction line. The solid lines show the value of $N\eta(\frac{1}{2}\pi,1)$ at the crossing points shown in Fig. 8. The convergence is not smooth, but the corrections to scaling are very small; notice the expanded vertical scale.

the other results indicate that the specific heat diverges with the conventional Ising exponent, $\alpha=0$, that the missing-row order parameter vanishes with the Ising exponent, $\beta=\frac{1}{8}$, and that the roughness parameter takes the universal KT value $K_G=\frac{1}{2}\pi$. The only quantity with an unusual value is the universal FSS amplitude of $\eta(\frac{1}{2}\pi,1)$. Along the entire roughening-induced deconstruction line I find $N\eta(\frac{1}{2}\pi,1)=1.03\pm0.03$; see Fig. 14. The accuracy in this quantity is relatively high, because corrections to scaling in this quantity are virtually absent.

One should wonder whether the Ising and roughening line really merge at $R\simeq 2$, or stay separate at an extremely close distance. Within the numerical accuracy they certainly merge. The S-T invariance discussed in the following section sheds more light on this and also on the scaling properties of the roughening-induced simultaneous deconstruction transition.

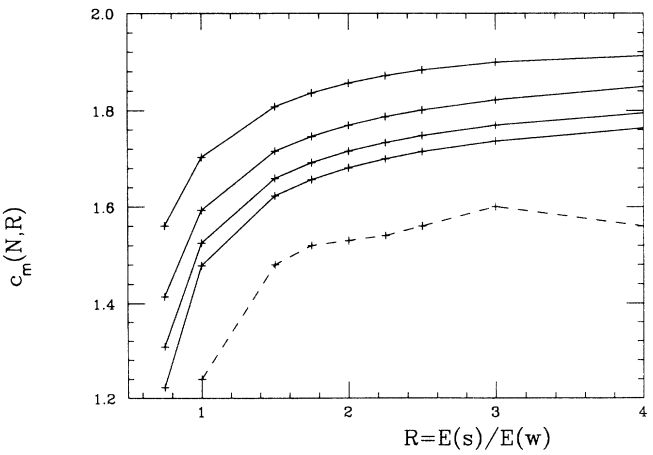

FIG. 13. Finite-size-scaling estimates for the central charge, $c_m(N,R)$, along the roughening-induced simultaneous deconstruction line at the location of the maxima in Fig. 12. The data at successive values $(N,N+1)-(3,4)$, (4,5), (5,6), and (6,7) converge smoothly towards the dashed line, which represents a power-law extrapolation.

IV. S-T INVARIANCE

The numerical results of Sec. III indicate that the roughening-induced deconstruction transition at zero chirality has central charge $c=\frac{3}{2}$. This is somewhat of a surprise. A conventional Ising transition has $c=\frac{1}{2}$, and a conventional roughening transition has $c=1$ (including the rough phase itself). It seems as if the Ising and roughening lines simply merge without a crossover to fundamentally different scaling properties. Also the numerical values for the critical exponents indicate that Ising and roughening critical behavior are simply superimposed.

In this section the argument of Sec. II, namely that roughening induces a simultaneous deconstruction transition, will be reformulated in terms of a Z_2-type invariance. I call this S-T invariance. It resembles supersymmetry, and provides insight into why the critical exponents do not seem to change. S-T invariance is likely to play a central role in future classification of this transition in terms of conformal field theory.

Moreover, at the end of this section we find that at zero chirality the four-state clock-step model is equivalent to an Ising model coupled to a planar model, of a type studied recently in the context of the fully frustrated XY model.[20]

Conformal field theories with $c>1$ typically involve an extra symmetry. In particular, $c=\frac{3}{2}$ is associated with supersymmetry.[30] A simple example of a transition with supersymmetry is the deconstruction transition inside the rough phase of simple cubic (sc) (110) facets. In Sec. II

this transition is described first in terms of a RSOS model with antiferromagnetic nearest-neighbor interactions, Eq. (2.2), and then in terms of a cell-spin model which is an Ising model coupled to a RSOS model, Eq. (2.3).

The four-state chiral clock-step model, Eq. (2.4), can be written in the form of Eq. (2.3) when chirality is absent, $\Delta=0$. In Eq. (2.4) and Figs. 3 the 4 possible top positions of the missing rows are represented by the angular variable θ. Choose an alternative representation in terms of two coupled Ising spins; $\theta=(0,\frac{1}{2}\pi,\pi,-\frac{1}{2}\pi)$ as $(S,T)=(++),(+,-),(-,-),(-,+)$. Equation (2.4) takes the form

$$Z=\sum_{\{S_r,T_r\}}\exp\left\{\sum_{\langle r,r'\rangle}[\tfrac{1}{2}K(T_rT_{r'}+S_rS_{r'})+QS_rS_{r'}T_rT_{r'}]\right\}\times Z_{6V}(\{S_r,T_r\},L) \tag{4.1}$$

with r and r′ nearest-neighbor sites. The 6V model describes the height fluctuations in the surface, and is defined on the joint lattice formed by the Bloch walls of both Ising models; bonds where S- and T-type Bloch walls overlap are excluded.

In the MR-reconstructed phase the magnetizations $\langle S\rangle=\langle T\rangle$ and the polarization $\langle ST\rangle$ are nonzero. When the magnetizations $\langle S\rangle=\langle T\rangle$ vanish the surface deconstructs. At $R\ll 2$ the two types of Ising spins are strongly coupled and their Bloch walls appear in pairs. These bound pairs represent the wall excitations of Fig. 3(b). In the DOF phase the polarization $\langle ST\rangle$ remains nonzero. When the polarization $\langle ST\rangle$ vanishes the surface roughens. This happens at a higher temperature, where the bound pairs of the two types of Bloch walls break up. At $R\simeq 2$ the two species of Bloch walls are weakly coupled. At $R\gg 2$ they repel each other, they do not form bound pairs anymore, and at T_c the magnetizations and polarization vanish simultaneously. The surface roughens and deconstructs simultaneously. Above T_c the two species of Bloch walls form an infinite large backbone lattice for the 6V arrows (which denote the change in height at these steps). At small values of L such a 6V model is certainly in its rough phase. Below T_c the surface is flat because the Bloch walls form only finite disconnected lattices for the 6V arrows (compare with Refs. 1 and 2).

Redefine the spins such that the 6V model arrows live on one type of Bloch walls only. This can be achieved in two ways: define $\sigma=ST$ and keep S or T. This choice gives rise to the S-T invariance. In the (σ,T) representation Eq. (4.1) takes the form

$$Z=\sum_{\{\sigma_r,T_r\}}\exp\left\{\sum_{\langle r,r'\rangle}[\tfrac{1}{2}KT_rT_{r'}+(\tfrac{1}{2}KT_rT_{r'}+Q)\sigma_r\sigma_{r'}]\right\}\times Z_{6V}(\{\sigma_r\},L)\,. \tag{4.2}$$

This can be rewritten as a RSOS model coupled to an Ising model, by combining the six-vertex arrows and σ spins into height variables, h_r. σ represents the parity, $\sigma_r=\exp(2\pi h_r)$, and the 6V arrow on each σ Bloch wall denotes whether the step is up or down, $dh=\pm 1$ [compare with Eqs. (2.1) and (2.2) in Ref. 1],

$$Z=\sum_{\{h_r,T_r\}}\exp\left\{\sum_{\langle r,r'\rangle}\{\tfrac{1}{2}K_tT_rT_{r'}+(\tfrac{1}{2}K_sT_rT_{r'}+Q)\times[1-2(h_r-h_{r'})^2]\}\right\}. \tag{4.3}$$

For simplicity L is set equal to $L=0$; L represents a next-nearest-neighbor interaction between the height variables.

Equation (4.3) is identical to (2.3), with one essential constraint: S-T invariance implies that $K_s=K_t=K$. In the alternate (σ,S) representation K_s and K_t are interchanged. S-T invariance represents the fundamental property that the height and reconstruction degrees of freedom cannot be disentangled. Recall from Sec. III that for sc (110) facets, interchanging S and T has the effect of disentangling the MR and roughening degrees of freedom. In sc surfaces K_s and K_t are not equal.

S-T invariance expresses the following symmetry property of MR reconstructed fcc (110) facets. Although we use a four-state clock variable to describe the reconstruction, the MR state is only twofold degenerate; $\theta=0,\pi$ are realized only at even heights, and $\theta=\pm\frac{1}{2}\pi$ only at odd heights (or vice versa). We could try to represent the reconstruction by an Ising variable. Equation (4.1) is a symmetric formulation, where we refuse yet to equate $\theta=0$ with $\theta=\frac{1}{2}\pi$ or with $\theta=-\frac{1}{2}\pi$. In the (σ,T) representation this symmetry is broken, $\theta=0$ is equated with $\theta=\frac{1}{2}\pi$, and $\theta=\pi$ with $\theta=-\frac{1}{2}\pi$. The (σ,S) formulation represents the opposite choice. S-T invariance expresses the absence of a preferred choice. The presence of a preferred choice would imply that $K_s\neq K_t$, and that it would be possible to disentangle the MR order parameter from the steps, like we did for the MR reconstructed sc (110) facets.

Consider the limit $K_s=0$ and $K_t\neq 0$. The Ising and roughening degrees of freedom decouple. At an appropriate choice of Q/K_t the Ising critical point is located inside the rough phase. This is a realization of a conformal field theory with the most simple type of supersymmetry, with central charge $c=1.5$. Supersymmetry means that an action is invariant under a continuous transformation that mixes fermion and boson degrees of freedom. It requires that the fermions and bosons are both massless. This applies to our problem, because an Ising model is a fermion theory (at its critical point the fermions are massless), and the RSOS model is a boson theory (in the rough phase the bosons are massless), but it holds only asymptotically, in the scaling limit, because it requires a continuum limit. This type of supersymmetry does not impose a connection between the Ising critical temperature and the roughening temperature. It does not restrict the value of the roughness parameter K_G, be-

cause in the rough phase the discreteness of the surface height variables is irrelevant; collectively they behave like Gaussian variables ϕ_r that take any real values (continuous height variables). The transformation $\phi_r \to \lambda\phi$ and $K_g \to \lambda^{-2}K_g$ leaves the Gaussian model invariant. Therefore supersymmetry does not exclude the existence of a reconstructed rough phase.

At small values of K_t the deconstruction transition remains in the same universality class as at $K_t=0$, because at $K_t=0$ the K_t interaction has an irrelevant scaling index, $y_t=3$ (the correlation functions of the MR and roughening degrees of freedom factorize). S-T symmetry implies the same type of behavior in the opposite limit, $K_s=0$. The line $K_s=K_t$ separates these two regions, and must be an unstable separatrix under renormalization transformations. According to the c theorem [31] the central charge of a higher-order critical point in a phase diagram must be larger than that of the lower-order critical points. This implies that $c \geq 1.5$ at the roughening-induced simultaneous deconstruction transition at $K_s=K_t$, and that this transition potentially belongs to a new type of universality class. Surprisingly, the numerical results of Sec. IV indicate that the central charge and the critical exponents hardly change.

S-T invariance has the character of a fermion-boson exchange similar to the above-mentioned supersymmetry; the S spins become part of the height variables while the T spins are extracted from the height variables. On the one hand S-T invariance is weaker than supersymmetry, because it is only a discrete Z_2-type invariance; only a subgroup of full supersymmetry. On the other hand it is stronger, because it is an exact invariance of the model which holds on the lattice, not only at T_c in the scaling limit but at all temperatures. This second aspect requires the roughening and deconstruction temperatures to coincide. The first aspect probably explains why S-T invariance has such a benign effect on the values of the critical exponents, but needs to be studied in more detail in the context of conformal quantum field theory. The question is whether in the scaling (continuum) limit full supersymmetry is restored. The presence of the marginal (sine-Gordon) operator in the roughening sector (the one that causes the KT instability) might change the properties of the field theory. Details of the critical properties of the transition, such as the precise shape of the specific-heat peak, must depend on this. I find numerical evidence for an Ising-type exponent $\alpha=0$, but the essential singularity (typical for conventional roughening transitions) is likely intertwined with this Ising behavior. At present my numerical accuracy is too limited to study this.

There is one quantity in the numerical study where the Ising and roughening degrees of freedom are required to truly mix, namely the step free energy $\eta(\frac{1}{2}\pi,1)$. It is defined as the difference in free energy of a semi-infinite strip with periodic and step-1-type boundary conditions, $\theta(x,y)=\theta(x+N_x,y)-\frac{1}{2}\pi$, $\quad h(x,y)=h(x+N_x,y)-1$. This quantity has an unusual universal finite-size-scaling (FSS) amplitude, $N\eta(\frac{1}{2}\pi,1)=1.03\pm0.03$; see Sec. IV. The question is whether this value is consistent with the other result that the Ising and roughening critical exponents hardly change. To make progress it is necessary to reformulate this boundary condition into the Ising-RSOS model formulation of Eq. (4.3). It is advantageous to do this in a general context.

Let us first focus on the reconstruction variables, and ignore the height degrees of freedom. The four-state clock-step model reduces then to the conventional Ashkin-Teller (AT) model,

$$\mathcal{H}_{\mathrm{AT}}=\sum_{i,j}[K\cos(\theta_{\mathrm{r}}-\theta_{\mathrm{r}'})+Q\cos(2\theta_{\mathrm{r}}-2\theta_{\mathrm{r}'})]\ . \tag{4.4}$$

The AT Hamiltonian is invariant under a set of global transformations, $R^{\theta}_{n,\pm}$, on all angle variables θ (see Table I). The generators are the rotation $\theta \to \theta+\frac{1}{2}\pi$, denoted by $R^{\theta}_{1,+}$, and the twist $\theta \to -\theta$, denoted by $R^{\theta}_{0,-}$.

Each $R^{\theta}_{n,\pm}$ is associated with a specific boundary condition. Consider semi-infinite lattices with as boundary condition in the finite lattice direction, $\theta(x,y)=\pm\theta(x+N_x,y)-n\frac{1}{2}\pi$. Each can be implemented in terms of periodic boundary conditions, but with modified interactions along a seam running across the entire lattice in the infinite lattice direction. At the seam the interactions are modified as

$$K\cos(\theta_L-R^{\theta}_{n,\pm}\theta_R)+Q\cos(2\theta_L-2R^{\theta}_{n,\pm}\theta_R)$$

with L and R nearest-neighbor spins, respectively, to the left and to the right of the seam. Spin L sees spin R rotated and twisted in accordance with the specific boundary condition. The location of the seam is arbitrary. It is gauge invariant, and can be moved to the right by performing the transformation $R^{\theta}_{-n,\pm}$ to all the spins between the old and the new location of the seam. Thus, all possible boundary conditions with gauge-invariant seams are characterized by the global transformations $R^{\theta}_{n,\pm}$ that leave the Hamiltonian invariant.

The (S,T) representations of these symmetry operators $R^{\theta}_{n,\pm}$ are listed in Table I. Exchanging the spin labels, $S \leftrightarrow T$, corresponds to the twist $R^{\theta}_{0,-}$, $\theta'=-\theta$. Reversal of one type of spin, $T'=-T$ and $S'=S$, corresponds to the rotational twist $R^{\theta}_{1,-}$, $\theta'=-\theta+\frac{1}{2}\pi$. The step free energy $\eta(\frac{1}{2}\pi,1)$, which is the focus of this discussion, is generated by the rotation $R^{\theta}_{1,+}$, and is a combination of these two operations, i.e., $S'=T$ and $T'=-S$.

The phase diagrams of the four-state clock-step model and the Ashkin-Teller model look very much alike. In the AT model two Ising lines merge into a single transition line, the so-called Baxter line, which plays the same role as the roughening-induced simultaneous deconstruction transition line in the four-state clock-step model. The critical behavior along the Baxter line can be understood as the result of the coupling of the S and T spins via the interaction Q, which has a marginal scaling index.[32] At the decoupling point, $Q=0$ (i.e., at $R=2$) the universal finite-size-scaling amplitudes follow easily in the (S,T) representation from the well-known results for the Ising model. For example, $R_{1,+}$ couples the two Ising models at the seam into a single Ising model of width $2N$ with antiperiodic boundary conditions. Therefore the interface free energy $\eta(1,+)$ scales as

TABLE I. Symmetry operations for the reconstruction variables in the four-state clock representation, θ, and the two Ising spin representations (S,T) and (σ,T).

Operator	θ representation	(S,T) representation	(σ,T) representation
$R^{\theta}_{1,+}$	$\theta'=\theta+\frac{1}{2}\pi$	$S'=-T$, $T'=S$	$\sigma'=-\sigma$, $T'=\sigma T$
$R^{\theta}_{2,+}$	$\theta'=\theta+\pi$	$S'=-S$, $T'=-T$	$\sigma'=\sigma$, $T'=-T$
$R^{\theta}_{0,-}$	$\theta'=-\theta$	$S'=T$, $T'=S$	$\sigma'=\sigma$, $T'=\sigma T$
$R^{\theta}_{1,-}$	$(\theta'+\frac{1}{4}\pi)=-(\theta+\frac{1}{4}\pi)$	$S'=S$, $T'=-T$	$\sigma'=-\sigma$, $T'=-T$

$$\eta(1,+)=(2N)f_i^a(2N)-2(Nf_i^p(N))=\frac{\pi}{4}N^{-1} \quad (4.5a)$$

with

$$f_i^p(N)=f_{\rm reg}-\frac{\pi}{6}cN^{-2} \quad (4.5b)$$

and

$$f_i^a(N)=f_{\rm reg}+\frac{\pi}{3}cN^{-2}\ , \quad (4.5c)$$

the FSS behavior of the free energy of an Ising model at criticality, on a semi-infinite strip of width N, with periodic (p) and antiperiodic (a) boundary conditions; $c=\frac{1}{2}$ is the central charge.

In the four-state clock-step model the Baxter line is replaced by the roughening-induced simultaneous deconstruction transition line. S-T invariance suggests that the critical properties along this line should be interpreted as the result of the interplay between the Ising and roughening variables in the Ising-RSOS model representation of Eq. (4.3). In the (σ,T) representation the interactions in the bulk have the form

$$\tfrac{1}{2}K(T_{\rm r}T_{\rm r'}+T_{\rm r}T_{\rm r'}\sigma_{\rm r}\sigma_{\rm r'})+Q\sigma_{\rm r}\sigma_{\rm r'}\ .$$

$R^{\theta}_{1,+}$ (see Table I) corresponds to the symmetry operation $\sigma'=-\sigma, T'=\sigma T$. To implement the $R^{\theta}_{1,+}$ boundary condition the interactions at the seam must be modified as

$$\tfrac{1}{2}K(\sigma_L-\sigma_R)T_LT_R-Q\sigma_L\sigma_R\ .$$

From the perspective of the σ spins the boundary conditions are antiperiodic. From perspective of the T spins the boundary condition is more complicated. It is a dynamic mixture of open, periodic, and antiperiodic boundary conditions: when the σ spins at both sides of the seam are aligned, $\sigma_L=\sigma_R$, the boundary condition looks open; when a σ-type Bloch wall follows the seam, $\sigma_L=-\sigma_R$, the boundary condition looks periodic if $\sigma_L=+1$ and antiperiodic if $\sigma_L=-1$.

Let us include now the height degrees of freedom. The step heights are restricted by the reconstruction variables: $d\theta=0,\pi$ implies no change in surface height, and $d\theta=\pm\frac{1}{2}\pi$ implies a step $dh=\pm1$. The four-state clock-step model is therefore invariant under the following global transformation of variables: $\theta\rightarrow\pm\theta+n\frac{1}{2}\pi$ and $h\rightarrow\pm h+m$, with the constraint that n and m must both be even or both be odd. This can be represented by the operator $R=R^{\theta}_{n,\pm}R^{h}_{m,\pm}$.

In Eq. (2.4) the step heights are represented by the arrows of the six-vertex model. The arrows live on the $d\theta=\pm\frac{1}{2}\pi$ walls of the four-state clock variables. In terms of these arrows, the $R^{h}_{m,\pm}$-type boundary condition implies that the net polarization in each slice of the cylindrical (semi-infinite) lattice is equal to m. For antiperiodic boundary conditions, $R^{h}_{m,-}$, the arrow on a step reverses its direction each time the step crosses the seam; and the polarization m is conserved only mod 2.

In the (σ,T) representation the six-vertex arrows live on the Bloch walls of the σ spins. Each σ type of Bloch wall is accompanied by an (odd) change in surface height. This implies that in the (σ,T) representation m is odd for antiperiodic $\sigma'=-\sigma$ boundary conditions, and m is even for periodic type $\sigma'=\sigma$ boundary conditions.

The step free energy $\eta(\frac{1}{2}\pi,1)$ is generated by $R=R^{\theta}_{1,+}R^{h}_{1,+}$. From the above discussion it follows that in the Ising-RSOS representation, Eq. (4.3), the interactions at the seam must be modified as

$$\tfrac{1}{2}K[\exp(i\pi h_L)-\exp(i\pi h_R)]T_LT_R-Q[1-2(h_L-h_R)^2]\ .$$

From the perspective of the RSOS model variables this is a simple step-1 boundary condition, $h(x,y)=h(x+N,y)+1$. From the perspective of the Ising spins, $T_{\rm r}$, this is a more complicated dynamic boundary condition: most of the time it looks like an open boundary condition, because in most configurations the steps will not coincide with the seam, i.e., $h_L=h_R$. Sometimes a step will follow a segment of the seam. Then it looks along this segment like a periodic boundary condition if h_L is even, and like an antiperiodic boundary condition if h_L is odd.

The seam is only gauge invariant when $K_s=K_t$. The operator $R^{\theta}_{1,+}$, which is used to move the seam, interchanges the K_s and K_t terms in the Hamiltonian. At $K_s\neq K_t$, the rotational invariance of the Hamiltonian, $\theta\rightarrow\theta+\frac{1}{2}\pi$, is lost, and $\eta(\frac{1}{2}\pi,1)$ cannot be generated by a gauge-invariant boundary condition. At $K_s\neq K_t$ the scaling properties of $\eta(\frac{1}{2}\pi,1)$ will be different.

I do not know how to proceed from here to obtain an exact result for $\eta(\frac{1}{2}\pi,1)$, but let us try the following assumption. The numerical results suggest that the Ising spins T and the height variables h basically decouple. Moreover, at the roughening temperature the density of steps in the RSOS model is still small, and the probability of them following segments of the seam is even smaller. Therefore treat the T spins as subject to an open boundary condition. This gives the estimate

$$\eta(\tfrac{1}{2}\pi,1)=[f_i^o(N)-f_i^p(N)]+\eta_{\mathrm{RSOS}}(1,N)$$
$$=\tfrac{5}{16}\pi N^{-1}=0.9817 \tag{4.6a}$$

with

$$f_i^0(N)=f_{\mathrm{reg}}-\frac{\pi}{24}cN^{-2} \tag{4.6b}$$

the finite-size-scaling behavior of an Ising model with open boundary conditions,[29] and

$$\eta_{\mathrm{RSOS}}(1,N)=\tfrac{1}{2}K_G N^{-1} \tag{4.6c}$$

the FSS behavior of the step free energy in the rough phase; with $K_G=\frac{1}{2}\pi$ at the roughening transition. This estimate, Eq. (4.6a), is remarkably close to the numerical value of Sec. III, $\eta(\frac{1}{2}\pi,1)=(1.03\pm0.03)N^{-1}$. It might be exact, or the contribution of the nonopen boundary segments is very small. We can conclude that the numerical value of the universal amplitude of $\eta(\frac{1}{2}\pi,1)$ is also consistent with simple superimposed Ising and KT roughening behavior.

The final issue of this section is to point out a connection between the four-state nonchiral clock-step model and frustrated XY models. Consider the Ising-RSOS model representation, Eq. (4.3). A duality transformation on the RSOS degrees of freedom maps Eq. (4.3) into an XY model coupled to an Ising model. Associate a step variable, $dh_{r,rl}=dh_{rl,r}=0,\pm1$, to each bond of the lattice and represent the constraint that along every closed path the sum of all the steps heights must be equal to zero as an integral over new periodic degrees of freedom $0\le\psi_R<2\pi$ located on the dual lattice site R,

$$\int_0^{2\pi}d\psi\exp[i\psi(dh_{1,2}+dh_{2,3}+dh_{3,4}+dh_{4,1})]$$
$$=2\pi\delta(dh_{1,2}+dh_{2,3}+dh_{3,4}+dh_{4,1})$$

where $r=1,2,3,4$ the four sites around the dual site R. The trace over the step variables, $dh_{r,r'}=0,\pm1$, factorizes, and after integrating them out they leave us with a model with only the angular variables ψ_R (on the dual lattice sites) and the Ising spins T_r (on the old lattice sites),

$$Z=\sum_{\{\psi_R,T_r\}}\prod_{\langle R,R'\rangle}\{\exp[\tfrac{1}{2}(K_s+K_t)T_rT_r'+Q]$$
$$+\exp[\tfrac{1}{2}(K_s-K_t)T_rT_r'-Q]2\cos(\psi_R-\psi_R')\}\ . \tag{4.7}$$

See, e.g., Ref. 33 for more details about this method of performing duality transformations.

The new model is similar in structure to models studied in recent years in the context of the fully frustrated XY model,[20] with phase diagrams of the same structure as Fig. 4, with an Ising and KT transition line that merge. Surprisingly the most recent numerical results suggest that in these models the central charge along the merged critical line differs from $c=1.5$; Granato *et al.*[20] find $c=1.5$ and a crossover to a first-order transition; Thijssen and Knops[20] find $c=1.66$. However, these models are slightly different from each other, and also from the one discussed here. Whether and how such small differences can influence the scaling behavior is a topic of future research. A related question is how S-T invariance generalizes to these frustrated XY models. S-T invariance applies to a larger set of Hamiltonians than the one of Eq. (4.7). For example, removal of the $dh=0,\pm1$ restriction in Eq. (4.3) does not destroy S-T invariance. The σ spins in Eq. (4.2), now defined as $\sigma_r=2\delta(h_r-h_{r'})-1$, still represent the presence of steps. The six-vertex model in Eq. (4.2) is replaced by a generalized vertex model with arrows of length $\pm1,\pm2,\pm3,\ldots$. Each arrow represents again the height change at the step. The arrows are restricted by the same rule as in the 6V model, namely that the total flux of arrows is equal to zero at each vertex. Perform to this generalized model the S-T transformation, $T\to\sigma T$ and $\sigma\to\sigma$, as described between Eqs. (4.1) and (4.2). This interchanges K_s and K_t, just like before, and leaves the Hamiltonian invariant.

V. THE STRONG CHIRALITY LIMIT

The structure of the phase diagram of the chiral clock-step model, Eq. (2.4), at strong chirality can be studied by the fermion method. This is the same technique as was used before in the theory of commensurate-incommensurate (C-IC) transitions in adsorbed monolayers. For a review see Ref. 24.

Consider values of Δ and Q in Eq. (2.4), where the energies of clockwise steps and walls, E_{cs} and E_w, both become much smaller than the energy of anticlockwise steps, E_{as}; see Eq. (2.5). Anticlockwise steps become frozen-out. Every bond of the lattice can only be in four states: empty, an up or down (clockwise) step, or a wall. This is actually the model for Au and Pt (110) proposed by Villain and Vilfan.[21] They pointed out that this two-dimensional statistical mechanical model is equivalent to the one-dimensional Hubbard model, but they did not fully pursue this equivalence.

Consider the quantum Hamiltonian

$$\mathcal{H}=\sum_{n=1}^{N}\{E_s(\sigma_n^+\sigma_n^-+\tau_n^+\tau_n^-)+(E_w-2E_s)\sigma_n^+\sigma_n^-\tau_n^+\tau_n^-$$
$$-t(\sigma_n^+\sigma_{n+1}^-+\sigma_{n+1}^-\sigma_n^++\tau_n^+\tau_{n+1}^-+\tau_{n+1}^-\tau_n^+)$$
$$-u_d(\sigma_n^+\tau_n^+\sigma_{n+1}^+\tau_{n+1}^++\sigma_n^-\tau_n^-\sigma_{n+1}^-\tau_{n+1}^-)\}\ , \tag{5.1}$$

where E_s is the energy of clockwise steps, and $\sigma_n^\pm$ and $\tau_n^\pm$ are two anticommuting fermion variables on each site of the chain: $\{\sigma_n^+,\sigma_m^-\}=\delta_{n,m}$, $\{\tau_n^+,\tau_m^-\}=\delta_{n,m}$, and $\{\sigma_n^\pm,\tau_m^\pm\}=0$. This Hamiltonian is related to the transfer matrix T of the four-state clock-step model in the strong chirality limit as $T\simeq\exp(-\mathcal{H}/k_BT)$. The ground-state energy of the quantum Hamiltonian, $\mathcal{H}$, is equivalent to the free energy. The quantum fluctuations are equivalent to thermodynamic fluctuations. The world lines of the fermions, in $(1+1)$-dimensional space time, are equivalent to the steps in the two-dimensional surface.

This equivalence is exact in the so-called time-continuum limit where $K_n\gg K_m$ and $Q_n\gg Q_m$; see Eq.

(2.4). In general it is approximate, but only in the sense that nonessential features, such as further than nearest-neighbor fermion interactions, are neglected. I will refrain from presenting a formal derivation. It is straightforward and completely analogous to earlier ones for models describing C-IC phase transitions in adsorbed monolayers.[24]

An up step is represented by the state (1,0), a down-step by (0,1), and a wall as a coinciding up and down step, (1,1). The hopping term represents the meander entropy of the steps. A hop occurs with probability $t \sim \exp[-E_k/k_BT]$, and creates a kink in the step. E_k is the kink energy. The dislocation operator creates excitations where two walls (or four clockwise steps with a total height change equal to zero) are annihilated or created at neighboring sites. The probability of this is related to the core energy of the dislocations, E_d, as $u_d = \exp[-E_d/k_BT] \sim t^2$.

This model is exactly soluble in the absence of dislocations, $u_d = 0$. It is the Hubbard model solved by Lieb and Wu.[22] In the continuum limit it is equivalent to the $n = 2$ Gross-Neveu model. This continuum limit is well understood; see Emery, Luther, and Peschel.[23] We need to reproduce this and incorporate dislocations. The following derivation is quite straightforward from the perspective of this earlier work on the Hubbard model. I follow the notation from Ref. 34. The derivation is somewhat technical, but the final result, Eqs. (5.20)–(5.22), can be understood on a much more qualitative level. Some readers might want to skip forward to Eq. (5.20).

After a Fourier transformation the Hamiltonian reads

$$\begin{aligned}\mathcal{H} = &\sum_k \{[E_s - 2t\cos(k)](\sigma_k^+\sigma_k^- + \tau_k^+\tau_k^-)\} \\ &+ \sum_{k,l,q} (E_w - 2E_s)\sigma_k^+\sigma_{k+q}^-\tau_l^+\tau_{l-q}^- \\ &- \sum_{k,l,q} 2u_d\cos(k+l)[\sigma_k^+\tau_l^+\sigma_{q-k}^+\tau_{-q-l}^+ \\ &+ \sigma_k^-\tau_l^-\sigma_{q-k}^-\tau_{-q-l}^-] \, . \end{aligned} \tag{5.2}$$

In the absence of dislocations $u_d = 0$ and interactions $E_w = 2E_s$, the fermions decouple. The model reduces to two independent tight-binding models with plane waves as eigenstates. Its phase diagram contains only two phases. The insulator state at $E_s > 2t$ represents the reconstructed flat phase, and the metal state at $E_s < 2t$ represents a rough deconstructed phase. In the latter the correlations decay as power laws, not only the roughening correlations but also those associated with the reconstruction degrees of freedom. In this phase the MR diffraction peaks have a power-law shape. The simultaneous roughening and deconstruction transition has the character of a Pokrovsky-Talapov (PT) transition with respect to both types of variables. (The scaling properties of PT transitions will be discussed below.) Dislocations and interactions complicate this simple phase diagram, however.

The continuum limit is constructed from the perspective of the metal phase of the two decoupled tight-binding models at $u_d = 0$ and $E_w = 2E_s$. Linearize the two energy bands at the Fermi surface. Define left and right moving fermion variables $\Psi_L(k)$ and $\Psi_R(k)$ for the linearized branches of the σ band, and $\Phi_L(k)$ and $\Phi_R(k)$ for those of the τ band. Shift these branches to the origin, $k \to k \pm k_F$. This leads to a Dirac-type Hamiltonian of the form

$$\mathcal{H} = \mathcal{H}_0 + \int dx [\lambda_B O_B(x) + \lambda_U O_U(x) - u O_D(x)] \tag{5.3}$$

with

$$\begin{aligned}\mathcal{H}_0 = &v \int dk [\Psi_R^+(k)\Psi_R^-(k) - \Psi_L^+(k)\Psi_L^-(k) \\ &+ \Phi_R^+(k)\Phi_R^-(k) - \Phi_L^+(k)\Phi_L^-(k)] \\ &+ \lambda \int dx [\rho_R^\sigma(x) + \rho_L^\sigma(x)][\rho_R^\tau(x) + \rho_L^\tau(x)] \, . \end{aligned} \tag{5.4}$$

v is the slope of the energy bands at the Fermi surface, $v = 2t\sin(k_F)$. The fermion density operators are related to the original density operators on the lattice as

$$\begin{aligned}\rho_n^\sigma &= \sigma_n^+\sigma_n^- - \frac{1}{\pi}k_F \simeq \rho_R^\sigma(x) + \rho_L^\sigma(x) \, , \\ \rho_n^\tau &= \tau_n^+\tau_n^- - \frac{1}{\pi}k_F \simeq \rho_R^\tau(x) + \rho_L^\tau(x) \, . \end{aligned} \tag{5.5}$$

λ, λ_B, and λ_U are renormalized coupling constants. For the following discussion it is only important that for small interactions they are proportional to $E_w - 2E_s$. u is the renormalized dislocation coupling constant. The three additional terms in Eq. (5.3) create excitations that are able to create energy gaps. All other higher-order excitations can only renormalize the coupling constants and are neglected.

The backward scattering operator

$$\begin{aligned}O_B(x) \sim &\Psi_R^+(x)\Psi_L^-(x)\Phi_L^+(x)\Phi_R^-(x) \\ &+ \Psi_L^+(x)\Psi_R^-(x)\Phi_R^+(x)\Phi_L^-(x) \end{aligned} \tag{5.6}$$

represents the process contained in the $\sigma_n^+\sigma_n^-\tau_n^+\tau_n^-$ interaction in Eq. (5.2) where fermions are scattered between opposite branches with $q \simeq 2k_F$. At $E_w = 2E_s$, where the two massless Dirac theories decouple, the critical dimension of the fermion operators Ψ and Φ is equal to $x_0 = \frac{1}{2}$. The critical dimension of the backward scattering operator O_B follows from power counting and is marginal at this decoupling point, $x_B = 2$. We will see below that this operator becomes relevant ($x_B < 2$) and creates a gap immediately at $E_w < 2E_s$. This gap is located at the Fermi surface and moves with the location of the Fermi surface, since $q = 2k_F$. These backward scattering excitations are associated with the roughening-type degrees of freedom, and this gap is associated with the flat phase where up-down steps condense into pairs and form wall excitations. From the Hubbard model perspective this gap is identified with a "spin-density wave."[22,23]

The umklapp operator

$$\begin{aligned}O_U(x) \sim &\Psi_R^+(x)\Psi_L^-(x)\Phi_R^+(x)\Phi_L^-(x) \\ &+ \Psi_L^+(x)\Psi_R^-(x)\Phi_L^+(x)\Phi_R^-(x) \end{aligned} \tag{5.7}$$

represents the process in the $\sigma_n^+\sigma_n^-\tau_n^+\tau_n^-$ interaction where fermions are scattered between opposite branches, with $q\simeq\pi$ using the $k\to k+2\pi$ periodicity in momentum space. Unlike backward scattering, this process is effective only when the energy bands are half filled, $k_F=\frac{1}{2}\pi$. Only then does it connect states with small energy. At the decoupling point the critical dimension of the umklapp operator follows again from power counting and is marginal, $x_U=2$. We will see below that this operator becomes relevant immediately at $E_w>2E_s$, and creates a gap at $k=\frac{1}{2}\pi$. This gap is associated with a higher-order reconstructed phase; a solid-type phase with a step excitation at every site and AF up-down order. The lattice-type cutoff in our cell-spin model is artificial, however, and therefore this higher-order phase with this artificial periodicity has no relevance for fcc (110) metal surfaces. From the Hubbard model perspective this gap is identified with a "charge-density wave."[22,23]

The dislocation operator obtains in the continuum limit the form

$$O_D(x)\sim \Psi_R^+(x)\Psi_L^+(x)\Phi_R^+(x)\Phi_L^+(x) + \Psi_R^-(x)\Psi_L^-(x)\Phi_R^-(x)\Phi_L^-(x) . \tag{5.8}$$

Also this operator is marginal at the decoupling point, $x_D=2$. We will see below that it becomes relevant immediately at $E_w>2E_s$, and creates a gap at the Fermi surface. We will associate this gap with the deconstructed fluid phase. It transforms the above "spin-density state" into the disordered flat fluid phase.

The next step is the conventional bosonization of the 1D fermion theory. One of the best discussions about this is the original paper by Tomonaga.[35] The two coupled Tomonaga-Luttinger models in $\mathcal{H}_0$ obtain the form

$$\begin{aligned}\mathcal{H}_0=\frac{2\pi}{L}\int dk\{&v[\rho_R^\sigma(k)\rho_R^\sigma(-k)+\rho_L^\sigma(-k)\rho_L^\sigma(k)\\&+\rho_R^\tau(k)\rho_R^\tau(-k)+\rho_L^\tau(-k)\rho_L^\tau(k)]\\&+\lambda[\rho_R^\sigma(k)+\rho_L^\sigma(k)]\\&\times[\rho_R^\tau(-k)+\rho_L^\tau(-k)]\} .\end{aligned} \tag{5.9}$$

The density operators do not commute anymore due to the introduction of the bottomless Dirac sea,

$$[\rho_{\beta_1}^{\alpha_1}(-k),\rho_{\beta_2}^{\alpha_2}(l)]=\frac{kL}{2\pi}\delta(\alpha_1,\alpha_2)\delta(\beta_1,\beta_2)\delta(k,l) . \tag{5.10}$$

The fermion operators are equivalent to string operators in terms of the density operators. This goes back to the work of Luther and Peschel[36] on the *XYZ* spin-$\frac{1}{2}$ quantum chain. Define

$$O_{n,m}^\alpha(x)=\exp[-\tfrac{1}{2}N\Theta_+^\alpha(x)-M\Theta_-^\alpha(x)] \tag{5.11}$$

and

$$\Theta_\pm^\alpha(x)=2\pi i\int_0^x dy[\rho_R^\alpha(y)\pm\rho_L^\alpha(y)] , \tag{5.12}$$

then[23,34,36]

$$\begin{aligned}&\Psi_R^+\sim O_{1,-1/2}^\sigma , \quad \Psi_R^-\sim O_{-1,1/2}^\sigma ,\\&\Psi_L^+\sim O_{-1,-1/2}^\sigma , \quad \Psi_L^-\sim O_{1,1/2}^\sigma ,\end{aligned} \tag{5.13}$$

and the same for the τ operators. This means that the backward scattering, umklapp, and dislocation operators can be represented as

$$\begin{aligned}&O_B(x)\sim O_{2,0}^\sigma(x)O_{-2,0}^\tau(x)+O_{-2,0}^\sigma(x)O_{2,0}^\tau(x) ,\\&O_U(x)\sim O_{2,0}^\sigma(x)O_{2,0}^\tau(x)+O_{-2,0}^\sigma(x)O_{-2,0}^\tau(x) ,\\&O_D(x)\sim O_{0,1}^\sigma(x)O_{0,1}^\tau(x)+O_{0,-1}^\sigma(x)O_{0,-1}^\tau(x) .\end{aligned} \tag{5.14}$$

Emery, Luther, and Peschel[23] found that the two types of boson variables decouple under the linear transformation

$$\begin{aligned}&\rho_\beta^d(k)=\tfrac{1}{2}\sqrt{2}[\rho_\beta^\sigma(k)+\rho_\beta^\tau(k)] ,\\&\rho_\beta^r(x)=\tfrac{1}{2}\sqrt{2}[\rho_\beta^\sigma(k)-\rho_\beta^\tau(k)] .\end{aligned} \tag{5.15}$$

Fortunately this remains true also in our case, in the presence of dislocations. The Hamiltonian decouples as

$$\mathcal{H}=\mathcal{H}_r+\mathcal{H}_d \tag{5.16}$$

with

$$\begin{aligned}\mathcal{H}_r=\frac{2\pi}{L}\int dk\{&(v-\tfrac{1}{2}\lambda)[\rho_R^r(k)\rho_R^r(-k)+\rho_L^r(-k)\rho_L^r(k)]\\&-\lambda\rho_R^r(k)\rho_L^r(k)\}\\&+\lambda_B\int dx[O_{2\sqrt{2},0}^r(x)+O_{-2\sqrt{2},0}^r(x)]\end{aligned} \tag{5.17}$$

and

$$\begin{aligned}\mathcal{H}_d=\frac{2\pi}{L}\int dk\{&(v+\tfrac{1}{2}\lambda)[\rho_R^d(k)\rho_R^d(-k)+\rho_L^d(-k)\rho_L^d(k)]\\&+\lambda\rho_R^d(k)\rho_L^d(k)\}\\&+\lambda_U\int dx[O_{2\sqrt{2},0}^d(x)+O_{-2\sqrt{2},0}^d(x)]\\&-u\int dx[O_{0,\sqrt{2}}^d(x)+O_{0,-\sqrt{2}}^d(x)]\end{aligned} \tag{5.18}$$

The ρ^d variables represent the surface reconstruction degrees of freedom. They count the number of steps irrespective of whether the step is up or down. They keep track of the winding number of the reconstruction θ variable in Eq. (2.4). The ρ^r variables represent the surface roughness degrees of freedom. They count the number of up steps minus the number of down steps. They keep track of the change in surface height.

Equations (5.17) and (5.18) can be rewritten as scalar field theories. Define scalar field variables and their conjugate momentum operators as[23,34,36]

$$\begin{aligned}&p^\alpha(x)=\frac{i}{2\pi}\frac{d\Theta_-^\alpha}{dx} ,\\&q^\alpha(x)=\frac{i}{2}\Theta_+^\alpha ,\end{aligned} \tag{5.19}$$

with $\alpha=r,d$. The Hamiltonians read

$$\begin{aligned}\mathcal{H}_r=\int dx&\left\{\frac{\pi}{2}v(p^r(x))^2+\frac{1}{2\pi}(v-\lambda)\left[\frac{dq^r(x)}{dx}\right]^2\right\}\\&+\lambda_B\int dx[O_{2\sqrt{2},0}^r(x)+O_{-2\sqrt{2},0}^r(x)]\end{aligned} \tag{5.20}$$

and

$$\mathcal{H}_d = \int dx \left\{ \frac{\pi}{2} v (p^d(x))^2 + \frac{1}{2\pi}(v+\lambda) \left[\frac{dq^d(x)}{dx} \right]^2 \right\} + \lambda_U \int dx [O^d_{2\sqrt{2},0}(x) + O^d_{-2\sqrt{2},0}(x)] - u \int dx [O^d_{0,\sqrt{2}}(x) + O^d_{0,-\sqrt{2}}(x)] . \quad (5.21)$$

The operators $O^{\alpha}_{N,M}$ are combinations of sine-Gordon and dislocation operators, and represent electric and magnetic charges in the Coulomb gas formulations of these models.[34,37]

The stability of the free scalar field theory, at $u=\lambda_B=\lambda_U=0$, with respect to the excitations with topological charge, $O^{\alpha}_{N,M}$, is determined by the value of the critical dimension $x^{\alpha}_{N,M}$ of these charges. The $x^{\alpha}_{N,M}$ vary continuously with the interaction parameter λ as[34]

$$x^{\alpha}_{N,M} = \frac{N^2}{4x^{\alpha}} + M^2 x^{\alpha} \quad (5.22)$$

with x^r a continuously increasing function of λ. At small λ, x^r behaves as $x^r \simeq \sqrt{(1-\lambda/v)}$. The critical exponents in the H^d sector vary in the same way, but x^d is a continuously decreasing function of λ because λ appears in H^d with a minus sign. At small λ, $x^d \simeq \sqrt{(1+\lambda/v)}$.

We are now ready to discuss the phase diagram of the chiral four-state clock-step model at strong chirality. The above derivation of the continuum limit, although straightforward, is quite technical, and not very transparent for those readers not familiar with the technique. Fortunately the results are easily understood qualitatively.

One of the major results is the decoupling of the roughening and reconstruction sectors in the continuum limit. This implies that from the large length scale perspective the two types of degrees decouple. Figure 15(a) shows the phase diagram of the roughening sector, Eq. (5.20), at a fixed value of the chirality. $\mathcal{H}^r$ is a sine-Gordon model just like the continuum limit of a conventional SOS model. The backward scattering operator is the sine-Gordon operator. According to Eq. (5.22), the critical dimension of O_B is equal to $x_B = 2/x^r$. At the repulsive side, $\lambda > 0$, O_B is irrelevant, $x_B > 2$, and we can ignore its excitations. So H^r behaves at $\lambda > 0$ like a free massless scalar field theory. This is the same as the metal phase in the fermion representation. This massless phase represents the rough phase, and it is located in the upper right corner of the phase diagram, Fig. 15(a). In this phase the only effect of the backward scattering operator is to renormalize the coupling constants, in particular λ.

The KT-type roughening transition takes place at the line $\lambda = 0$ where the backwards scattering operator becomes relevant, $x_B < 2$. At the attractive side, $\lambda < 0$, the surface is flat. The correlation length is finite, because the backward scattering excitations create a gap at the Fermi surface.

In Fig. 15(a) the line $\lambda = 0$ bends to the left. This is because $E_w - 2E_s$ is the bare coupling constant, unlike λ, the renormalized one. Assign extra labels to the λ's in Eqs. (5.20) and (5.21). In lowest order $\lambda_r = \lambda_d$ and both are simply proportional to $E_w - 2E_s$, but higher-order excitations renormalize the λ's. For increasing temperature, at fixed $E_w - 2E_s$, λ_r increases (becomes less attractive). For example, anticlockwise (AC) steps appear in terrace-type C-AC step pair excitations; see Fig. 16(a). Such an excitation is small in size (has a short lifetime) because the AC step has a large mass. Moreover, it requires that there is enough empty space between steps to fit in between. Under renormalization (at larger length scales) it vanishes, but leaves an effective repulsion between the steps. See Ref. 24 for a more-detailed discussion of this type of effect. So for increasing temperature λ_r increases. This implies that the $\lambda_r = 0$ line bends to the left in Fig. 15(a).

A different type of roughening transition occurs at fixed $\lambda > 0$ at increasing temperature. This roughening transition has the character of a Pokrovsky-Talapov (PT)

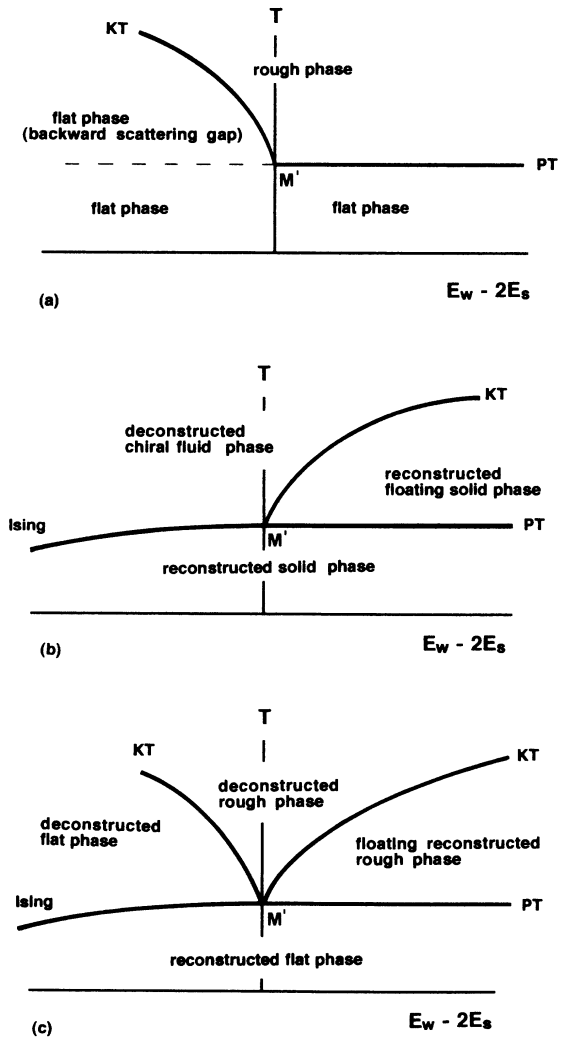

FIG. 15. Schematic phase diagram of the four-state chiral clock-step model at strong chirality from the continuum limit formulation: (a) the roughening sector, from Eq. (5.20); (b) the deconstruction sector, from Eq. (5.21); and (c) the combined full phase diagram.

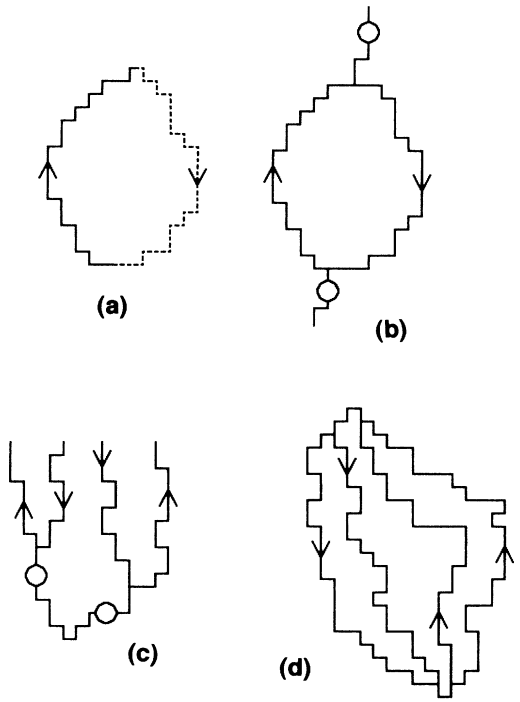

FIG. 16. Typical step and wall configurations: (a) a clockwise (C) step becomes an anticlockwise (AC) step when it turns backwards to form an elementary terrace excitation; (b) a wall splits temporarily into a C up step and a C down step; (c) an elementary dislocation creates two walls which later both split up into two steps; (d) a dislocation pair creates a local structure consisting of four C steps (two up steps and two down steps).

transition. This is the metal-insulator-type transition associated with the bottom of the energy band in the lattice model and takes place when $E_s = 2t$ [see Eq. (5.2)].

As mentioned above, it is possible to understand this phase diagram, Fig. 15(a), on a less technical level. The decoupling of the roughening and deconstruction sectors, $\mathcal{H}_r$ and $\mathcal{H}_d$, in the continuum limit tells us to ignore the reconstruction aspect $d\theta$ of steps and walls for the discussion of the roughening of the surface. This means that with respect to the roughening degrees of freedom wall excitations do not exist (they are invisible because they do not change the height), and that clockwise and anticlockwise steps are indistinguishable. This suggests that as far as the roughening degrees of freedom are concerned we can replace the full model by a conventional SOS model. $\mathcal{H}_r$ has indeed the structure of a sine-Gordon model, i.e., the proper continuum limit of a SOS model. But this must be too simplistic, because topological constraints imposed by the θ variables remain. When a step turns backwards it changes from a clockwise into an anticlockwise step. By freezing out the anticlockwise steps, we have frozen out the possibility for steps to turn backwards. They cannot close on themselves to create small terrace-type droplets, see Fig. 16(a), where the height changes by 1. This explains the PT nature of the roughening transition at the repulsive side of the phase diagram. Disallowing turn-back excitations in a conventional SOS model has indeed the effect of replacing the KT-type roughening transition by a PT transition; the SOS model reduces to a tight-binding-type free-fermion model.

The backward scattering operator O_B represents a different type of excitation which resembles a simple terrace droplet. A wall excitation is invisible from the roughening perspective, but can split into an up step and a down step, and later recombine; see Fig. 16(b). In the presence of a background sea of walls, when the wall free energy has vanished, these excitations are governed by the step free energies only, and therefore behave like in a conventional SOS model (conventional sine-Gordon model) and should induce a conventional KT transition. Indeed, we will see next that the walls form such a background sea at the attractive side, $\lambda_d < 0$ [everywhere to the left of the KT transition line and above the Ising line in Fig. 15(b)].

The Hamiltonian $\mathcal{H}_d$ of the reconstruction sector contains the umklapp and the dislocation operator. At the decoupling point both are marginal. They are relevant at opposite sides: O_U is relevant when the steps repel each other, $\lambda_d > 0$. Its critical dimension is equal to $x_U = 2/x^d$. O_D is relevant at the attractive side, $\lambda_d < 0$. Its critical dimension is equal to $x_D = 2x^d$.

The umklapp excitations create a gap in the energy spectrum, but only at half-filling, $k_F = \frac{1}{2}\pi$. At all other filling factors the umklapp operator is ineffective. As mentioned above, the umklapp gap represents a higher-order reconstructed phase and is an artifact of the lattice cutoff. The corner of the phase diagram where this phase is located at very strong chirality is not of interest to us. Consider filling factors close to the bottom of the band, where we can ignore O_U. Figure 15(b) shows the phase diagram of the reconstruction sector, again at a fixed value of the chirality. It contains a reconstructed solid, IC floating solid, and chiral deconstructed fluid phase. O_D is irrelevant in the upper right corner of the phase diagram (the repulsive side). There the reconstruction sector is in the massless phase of the scalar free-field theory (the metal phase in the fermion representation). The reconstruction diffraction peak has a power-law shape and is shifted to an IC position proportional to the steps density. The phase boundary between the floating solid and reconstructed solid phase is a PT transition. Like the roughening sector this transition takes place when the Fermi level drops below the bottom of the band in the lattice model.

The dislocation operator represents the excitations where two walls are created from the vacuum; see Fig. 16(c). Dislocations become relevant at the line $\lambda_d = 0$. At this line the floating MR solid melts into a chiral deconstructed fluid; the MR diffraction peak becomes Lorentzian but remains shifted. The same argument above, which predicts that the line $\lambda_r = 0$ bends to the left in Fig. 15(a), implies that the line $\lambda_d = 0$ bends to the right in Fig. 15(b).

Finally, the transition between the MR solid and chiral deconstructed fluid is an Ising transition. This is not obvious in the continuum theory. Consider the fermion Hamiltonian, Eq. (5.1), in the limit of strong attraction

$E_w - 2E_s \ll 0$. Only the states $(\sigma,\tau)=(0,0)$ and (1,1) are allowed. Define new fermion operators $a^{\pm}=\sigma^{\pm}\tau^{\pm}$. Then the Hamiltonian reduces to the conventional Ising model (quantum spin-$\frac{1}{2}$ XY model),

$$\mathcal{H}=\sum_{n=1}^{N}\{E_w a_n^+ a_n^- - t'(a_n^+ a_{n+1}^- + a_{n+1}^+ a_n^-) - u_d(a_n^+ a_{n+1}^+ + a_n^- a_{n+1}^-)\} . \quad (5.23)$$

In the Hamiltonian of Eq. (5.1) only steps can hop. Therefore the hopping term in Eq. (5.23) is a second-order process where the wall splits into an intermediate state with two steps, and is of order $t' \sim t^2/(2E_s - E_w)$.

Figure 15(c) shows the full phase diagram of the four-state clock-step model at strong chirality. It follows by superposition of the phase diagrams of the roughening and reconstruction sectors, Figs. 15(a) and 15(b). One important feature is that the PT transition lines and also the multicritical point M' of the roughening and reconstruction sectors coincide. Consider Eq. (5.1): In the tight-binding model limit, $u_d=0$ and $E_w-2E_s=0$, the two PT transitions are already present, and they coincide. The step interactions and dislocations do not alter this part of the phase diagram. They do not renormalize the energy levels at the bottom of the energy band, because the density of steps vanishes at the PT transition. Therefore the location of the PT transition lines does not change with the inclusion of interactions and dislocations.

VI. THE GLOBAL PHASE DIAGRAM

In the preceding sections we studied the chiral four-state clock-step model, first at zero chirality and then at strong chirality. We obtained a good understanding of both limits; see Figs. 4 and Fig. 15(c). From this it is possible to propose the structure of the global phase diagram and to discuss how recent experimental results for Au and Pt (110) relate to this. Figure 18 shows the most likely structure. Temperature is measured in units of the average step energy, $E_s=\frac{1}{2}(E_{cs}+E_{as})$. $R=E_w/E_s$ is the ratio between the wall and step energy. Chirality varies along the $\Delta=E_{cs}-E_{as}$ axis [defined slightly differently from Eq. (2.4)].

Paths of type 3 are located at the $R<2$ side of the phase diagram. An Ising-type deconstruction transition is followed by a KT-type roughening transition. Chirality does not affect this. The only new aspect is a possible shift in the MR diffraction peak at nonzero chirality. This will be discussed below.

Paths of type 4 are located at the $R>2$ side of the phase diagram. The line in Fig. 18 marked as L is a line of Lifshitz points. The sequence of phase transitions and their nature changes at this line. We will distinguish between paths of type 4a (at the small chirality side of L) and type 4b (at the large Δ side of L).

Along paths of type 4a the surface deconstructs and roughens simultaneously. The flat reconstructed solid phase transforms directly from the MR-reconstructed flat phase into the rough deconstructed chiral fluid phase. The scaling properties of this phase transition are the same as at zero chirality, apart from one new aspect. The missing-row diffraction peak starts to shift at T_c at the high-temperature side; the reconstruction variables undergo a so-called chiral melting transition. The properties of this transition will be explained below.

Along a path of type 4b the surface roughens and deconstructs simultaneously via a Pokrovsky-Talapov (PT) -type transition. These are two independent but simultaneous PT transitions, one with respect to the roughening and another one with respect to the reconstruction variables. The surface enters a phase which is rough and simultaneously a floating incommensurate (IC) solid with respect to the reconstruction variables. This means that not only the roughening-type correlations but also the reconstruction-type correlations decay as power laws. The MR diffraction peak starts to shift at the PT transition. At a higher temperature the reconstruction degrees of freedom melt via a conventional KT transition. The floating IC reconstructed rough solid melts into the rough deconstructed chiral fluid phase. This sequence of transitions follows from the fermion analysis at strong chirality, discussed in Sec. V. More details will follow below.

The structure of the phase diagram, Fig. 17, is based on the detailed knowledge of the two limit cases discussed in the preceding sections, and on the analogy with the phase diagram of conventional chiral clock models (the ones that describe IC monolayers). The major uncertainty is the existence and precise location of the Lifshitz line L that emerges from the multicritical point M' at strong chirality. Does the Lifshitz line exist, or does it coincide with the line $M-M'$; i.e., do paths of type 4a exist, or is there an immediate crossover to paths of type 4b at nonzero chirality? Moreover, the scaling behavior at the Lifshitz points must be interesting. Lifshitz points exhibit anisotropic scaling behavior. At this stage I have no information about the scaling behavior along the Lifshitz line.

Additional numerical work will be needed to settle

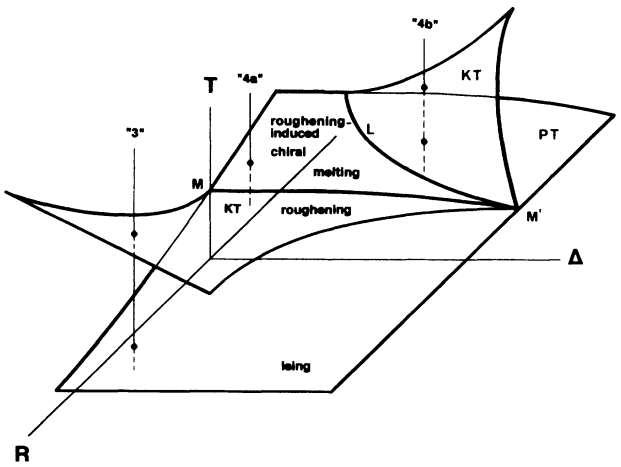

FIG. 17. Schematic structure of the full phase diagram of the four-state chiral clock-step model, with $R=E_w/E_s$, $\Delta=E_{ac}-E_c$, and temperature T measured in units of the step energy E_s.

these questions. At present this is beyond the scope of the type of finite-size-scaling (FSS) analysis presented in Sec. III. The maximum attainable strip width is too small. The numerical FSS results at nonzero chirality presented below are of limited value.

This uncertainty about the existence of the Lifshitz line exists also in conventional chiral clock models. Numerical evidence for the three-state chiral clock model (the most extensively studied version) supports the existence of a Lifshitz point, but the few exact analytical results that address this issue can be interpreted as supporting both possibilities.[24] It is fair to say that the Lifshitz point issue has not been settled beyond dispute in the three-state chiral clock model. At this stage we cannot expect to do better in the four-state clock-step model which is a more-complex model.

Pt(110) and Au(110) follow specific paths through the phase diagram, Fig. 17. The values of R and Δ for these surfaces can be determined in principle from microscopic energy considerations, such as the embedded-atom method[25] and pseudopotential method.[39] Unfortunately no reliable estimates exist yet. Instead, we will discuss the experimental signature of each type of path and determine which one is consistent with the experimental evidence.

The scaling properties of the phase transitions and the appearance of a shift in the MR-type diffraction peak are the most important experimental signatures. At low temperatures, in the MR-reconstructed flat phase, the MR peak is located at the commensurate position, but it must start to shift at some temperature, because the high-temperature rough deconstructed phase has the character of an incommensurate (IC) fluid with respect to the reconstruction degrees of freedom.

Clockwise and anticlockwise steps have a different microscopic structure, and therefore a different energy; $\Delta \neq 0$. The high-temperature deconstructed rough phase contains more clockwise than anticlockwise steps. Therefore the clock variable θ rotates across the surface in the direction perpendicular to the missing rows with a period incommensurate with the lattice periodicity. Loosely speaking, Q is proportional to the difference in density of clockwise and anticlockwise steps. Q is actually smaller, because specific types of excitations, such as the dislocations, create small-scale structures that do not contribute to the large-scale modulation. For example, the reconstructed solid phase contains "droplet" excitations as shown in Fig. 16(d), but the pitch remains zero, $Q=0$, because the long-range θ order is preserved. The proper definition of Q^{-1} is in terms of correlation functions such as

$$G(x,y)=\langle \exp\{i[\theta(x+x_0,y+y_0)-\theta(x_0,y_0)]\}\rangle \sim \exp[-r/\xi+iQx] \tag{6.1}$$

with $r^2=x^2+ay^2$, a is the lattice anisotropy parameter, and the missing rows are running parallel to the y direction. Scattering experiments measure the Fourier transform of these types of correlation functions. The incommensurability is characterized by the pitch Q, and reveals itself in scattering experiments as a shift in the liquidlike MR diffraction peaks.

In certain cases an IC fluid phase contains sharp boundaries, so-called disorder lines, where Q locks in to a commensurate value, and the fluid becomes commensurate. An example is the disorder line in the ANNNI model (which describes IC adsorbed monolayers close to a twofold-degenerate commensurate ground state),[24] where Q remains strictly equal to zero at small chirality until the disorder line is crossed. In other cases, such as the fluid phase in the three-state chiral clock model, such a disorder line is absent. But there the concept of a chiral fluid becomes meaningless for most practical purposes when the periodicity Q^{-1} becomes larger than the correlation length ξ. At $Q^{-1}\sim\xi$ the shift in the diffraction peak becomes equal to its width. The line $Q^{-1}\sim\xi$ plays a role similar to that of a disorder line.

The four-state chiral clock-step model contains a disorder line at the $R<2$ side of the phase diagram (paths of type 3). I did not check this numerically, but its existence becomes quite apparent from the one-dimensional (1D) version of the model. The 1D model lacks a phase transition. The deconstructed rough fluid phase extends all the way to $T=0$. The transfer matrix of this very simple, and its leading (λ_0) and next leading (λ_1) eigenvalue can be obtained analytically. Their ratio yields the so-called mass gap, $m=\ln(\lambda_0/\lambda_1)$. The real part of m is inversely proportional to the correlation length ξ. m is a complex number if the fluid is incommensurate, $m=\ln(\lambda_0/\lambda_1)=\xi^{-1}+iQ$. The fluid becomes incommensurate when λ_1 becomes complex. (λ_0 is always real.) In the 1D model the pitch Q becomes nonzero immediately at $\Delta>0$ at the side of the phase diagram with paths of type 4 in the 2D model. At the side with paths of type 3, however, m remains real at small chirality. This implies the presence of a disorder line at this side of the phase diagram in the 1D model. There is no reason to expect that this is different in the 2 D model.

We will now discuss the characteristic behavior along the various paths through the phase diagram. Consider paths of type 4*b*. The decoupling of the reconstruction and roughening fluctuations in the continuum limit at strong chirality (Sec. V) implies the following behavior. The MR peak starts to shift at the Pokrovsky-Talapov (PT) transition. In the rough deconstructed floating IC solid phase, between the PT and KT line, the steps form a meandering striped structure. They run parallel along the MR direction across the entire lattice (dislocations only occur in bound pairs). At each step the reconstruction variable θ rotates clockwise by one unit $d\theta=\frac{1}{2}\pi$. The step heights dh are randomly correlated such that the height-height correlation function diverges logarithmically,

$$\langle (h_{r+r_0}-h_{r+r_0})^2\rangle \simeq \frac{1}{\pi K_G}\ln(|r|)\ . \tag{6.2}$$

The reconstruction-type correlation functions decay as power laws, e.g.,

$$G(x,y)=\langle \exp\{i[\theta(x+x_0,y+y_0)-\theta(x_0,y_0)]\}\rangle \sim \exp[iQx]r^{-2x_\theta}\ . \tag{6.3}$$

The critical exponent x_θ varies continuously inside the rough floating IC solid phase. At the PT transition the roughening and reconstruction degrees undergo a simultaneous but independent conventional PT transition. x_θ takes the universal value $x_\theta=1$ (this follows from the free fermion model), Eq. (5.1), at $E_w=2E_s$ and $t=u_d=0$, which becomes exact in the limit where the step density vanishes, i.e., at the PT transition; and is in complete analogy with the theory of commensurate incommensurate phase transitions in adsorbed monolayers. The pitch vanishes at the PT transition as $Q\sim|T-T_c|^{1/2}$. Define the pitch critical exponent x_Q as $Q\sim\xi^{-x_Q}$. The value $x_Q=\frac{1}{2}$ is inconsistent with the experimental evidence for Pt(110).

Another aspect that is missing in the experimental evidence for Pt(110) is the anisotropic scaling behavior typical for PT transitions. The correlation length in the direction along the MR grooves diverges as $l_\parallel\sim|T-T_{\rm PT}|^{-1}$ while in the direction orthogonal to the MR grooves it diverges as $l_\perp\sim|T-T_{\rm PT}|^{-1/2}$. The diffraction line shape becomes anisotropic at the PT-type roughening-induced simultaneous deconstruction transition.

At higher temperatures the reconstruction degrees of freedom melt at the KT transition. Pairs of dislocations shown in Fig. 16(d) unbind. The line shape of the MR peaks changes from power law to Lorentzian.

Consider paths of type 3. The surface deconstructs via a conventional Ising transition, followed by a KT-type roughening transition at higher temperatures. Chirality does not affect this. The only question concerns the behavior of the pitch Q at strong chirality and $R\simeq 2$. The question arises whether this shift starts at the roughening transition, the Ising transition, or somewhere in the DOF phase at a disorder line. At small chirality or $R\ll 2$ the MR diffraction peak does not shift at all (when there exists indeed a disorder line), or not sufficiently to be meaningful (when the correlation length is smaller than the pitch, $\xi<Q^{-1}$).

In the DOF phase the surface contains a disordered array of wall excitations. Walls have a topological charge $d\theta=\pi$. In cases where they are sharp objects, as shown in Fig. 3, it is meaningless to distinguish between whether θ rotates clockwise or anticlockwise across the wall. So sharp walls do not contribute to the peak shift, and in the limit $R\ll 2$ where the steps are frozen out and the walls are sharp Q must remain equal to zero in the DOF phase at all values of Δ.

Along paths of type 3 close to $R=2$ in the limit of strong chirality this becomes less clear. There the walls can be thought of as bound states of two clockwise steps (an up and down step, or a down and up step). At large length scales it is still meaningless to distinguish between whether θ rotates clockwise or anticlockwise over π. But at resolutions better than the wall width it becomes visible that θ rotates clockwise.

Insight into this can be obtained again from a one-dimensional (1D) version of the model. Consider the 1D four-state chiral clock-step model at strong chirality, with a modification to ensure that it describes the DOF phase (instead of the deconstructed rough phase). Consider a 1D lattice with on each site a $\theta=(0,\frac{1}{2}\pi,\pi,-\frac{1}{2}\pi)$ variable. Assume that only $d\theta=\pi$ walls are allowed, but give them a fixed width l_w, and let inside the wall θ be rotated clockwise by $\frac{1}{2}\pi$. E_w is the wall energy (the energy of the bound step pair). This model describes a 1D version of the DOF phase in the limit of strong chirality, and can be solved exactly. It is easy to calculate the MR-type correlation function Eq. (6.1). Again, the transfer matrix is simple. The ratio of the leading and next-leading eigenvalues yields the mass gap, $m=\ln(\lambda_0/\lambda_1)=\xi^{-1}+iQ$. λ_1 is real at low temperatures, but becomes complex at $w_d\simeq l_w^{-1}$ [with $w=\exp(-E_w/k_BT)$]. This means that the DOF phase is commensurate at low temperatures ($Q=0$), until a sharply defined temperature, a disorder point (like the disorder line above), where the DOF fluid becomes incommensurate ($Q\neq 0$). At the disorder point the correlation length $\xi\simeq 2w$ is smaller than the wall width $\xi\simeq 0.7l_w$. In the commensurate DOF fluid, at lower temperatures, the correlation length is larger.

Consider a second model, a 1D BCSOS model, where at $T=0$ the surface is in the MR-reconstructed ground state. At $T>0$ only the clockwise step excitations of Fig. 3(c) are allowed, and they only appear in pairs (up-down or down-up pairs), at a fixed distance l_w. This condition ensured again that this model describes the DOF fluid at strong chirality. Also this mode lis exactly soluble. The results are the same. Again the fluid remains commensurate below a sharply defined disorder temperature, and again the correlation length at the disorder temperature is slightly smaller than the wall width. The advantage of this second model is that the correlation function

$$G(x,y)=\langle\exp\{iq[h(x+x_0)-h(x_0)]\}\rangle\ , \tag{6.4}$$

which is more directly related to the experiments than Eq. (6.1), is directly accessible. The scattering experiments measure the Fourier transform of this correlation function. The MR diffraction peak does not shift until the disorder temperature.

It is reasonable to conclude that also in the two-dimensional DOF fluid phase the pitch remains zero as long as the correlation length is larger than the wall width. ξ diverges at the Ising-type deconstruction transition, but the wall width l_w, is finite. Therefore I do not expect the peak shift to start at the Ising-type deconstruction transition. At a higher temperature the surface roughens. This KT-type transition is driven by the terrace-type step excitations shown in Fig. 16(b) as explained in Sec. V. A wall splits temporary into two clockwise steps. This implies that close to the roughening transition l_w takes over the role of correlation length and diverges. ξ remains finite, because it represents the correlation length associated with the θ variables, which do not become critical (ξ is a measure of the average distance between the walls in the disordered array of walls, which form the background, the "vacuum," for these terrace-type excitations). This implies that close to the roughening transition l_w becomes larger than ξ. The above 1D results suggest that the DOF fluid is then in-

commensurate, and the MR diffraction peak is shifted. I expect that Q becomes nonzero at a disorder line inside the DOF phase, located at $l_w \simeq \xi$.

Consider a path of type 4*a*. The peak starts to move immediately at the roughening-induced simultaneous deconstruction transition. Define the pitch critical exponent x_Q as $Q \sim \xi^{-x_Q}$. At the IC melting transition the correlation length ξ and the IC wavelength Q^{-1} diverge simultaneously. By definition, Q vanishes at T_c as $Q \sim \xi^{-x_Q}$. The scaling properties at a chiral melting transition are determined by the value of x_Q.[38,24] If $1 < x_Q < 2$, it is clear that all critical exponents must remain the same as at $\Delta = 0$, because then the correlation length diverges slower than the wavelength Q^{-1}, and in the scaling limit the correlated spins are unaffected by the periodicity. At best the wavelength Q^{-1} acts as a temperature-dependent effective finite-size (FS) cutoff.[24] If $x_Q = 1$ it is not clear why the critical exponents should not change. Nevertheless, numerical evidence for the chiral three-state clock model supports a value $x_Q = 1$ and no change in the exponents.[24]

Assume that also in the chiral four-state clock-step model $x_Q = 1$, and that all critical exponents remain the same as at $\Delta = 0$. This implies a linear vanishing of the misfit $Q \sim |T - T_c|^{x_Q/y_T} \sim |T - T_c|$. This is remarkably consistent with the observations of Robinson *et al.* for Pt(110): they find that the intensity of the half-order peak scales as $|T - T_c|^{2\beta}$ with $\beta \simeq 0.11$, and that the peak width scales as $\xi \sim |T - T_c|^{y_t}$ with $y_T \simeq 1.05$, both consistent with the above numerical results at $\Delta = 0$, and they observe a linear vanishing of the misfit.

To check whether indeed $x_Q = 1$ and the critical exponents do not change in the four-state chiral clock-step model, I calculated the pitch Q numerically with the same FSS method as described in Sec. III. Q is obtained from the complex part in the next-leading eigenvalue of the transfer matrix, λ_1, for periodic boundary conditions, $m + iQ = \ln(\lambda_0/\lambda_1)$. This "mass gap" m is dual to the interface free energies η of Section III. Recall that the η's are nonzero in the MR-reconstructed phase and vanish in the rough deconstructed phase. The mass gap behaves in the opposite way, m is inversely proportional to the correlation length in the deconstructed rough phase, and vanishes in the MR phase.

A couple of technical comments are in order. The next-to-leading eigenvalue of the transfer matrix becomes complex at $\Delta \neq 0$ only if the "time"-evolution direction is chosen to be perpendicular to the missing rows, the x direction in Eq. (6.1). In the calculations of Sec. III the state in each "time" slice is represented by a q^N-dimensional vector, with $1 \leq q \leq 6$ the six possible states of each vertical bond (a wall, a clockwise or anticlockwise up or down step, or nothing). In this representation the absolute value of the reconstruction variable θ is not represented, and therefore it does not contain the complex eigenvalue which keeps track of the average winding number in θ. Therefore I enlarged in this calculation the state vector by a factor 4, and stored the value of θ between two specific vertical bonds. Fortunately the maximum obtainable strip size remained $N_m = 7$.

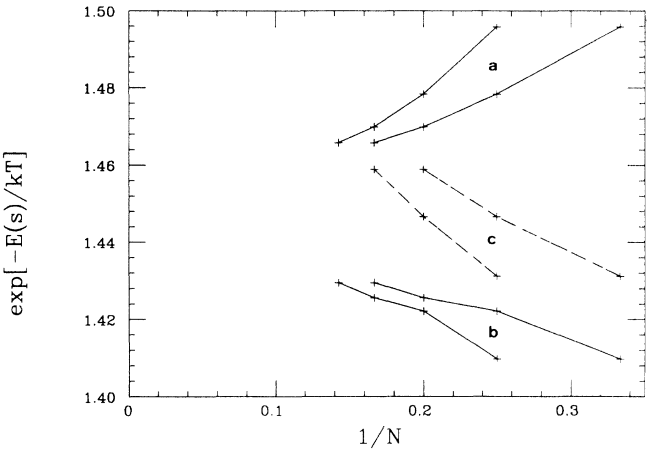

FIG. 18. The crossing points at $R = 3.0$ and $\Delta = 0.25$ of (a) the interface free energy $\eta(\pi, 0)$; (b) the interface free energy $\eta(\frac{1}{2}\pi, 1)$; and (c) the mass gap m. For each quantity two curves are shown: the crossing points as function of N and $N+1$.

At $\Delta \neq 0$ the lattice isotropy is lost. Therefore the simple relations between the universal FSS amplitudes and the critical dimensions of the operators that generate the specific boundary conditions (the η's) or the order parameter (the mass gap) are lost as well. Only the crossing point analysis of Sec. III can still be applied.

I limited my analysis to $R = 3$. Closer to the multicritical point at $R = 2$, crossover scaling behavior confuses the issue. At large values of R an Ising-type critical line (which is of no interest to the MR reconstruction) emerges from the AF side of the phase diagram and confuses the issue.

At $R = 3.0$ and $\Delta = 0.25$ the crossing points of $N\eta(\pi, 0)$, and $N\eta(\frac{1}{2}\pi, 1)$ clearly indicate convergence to a different estimate for the critical point than the crossing points of the mass gap, Nm (see Fig. 18). This indicates the presence of two transitions; we must have passed the Lifshitz line and crossed over to paths of type 4*b*.

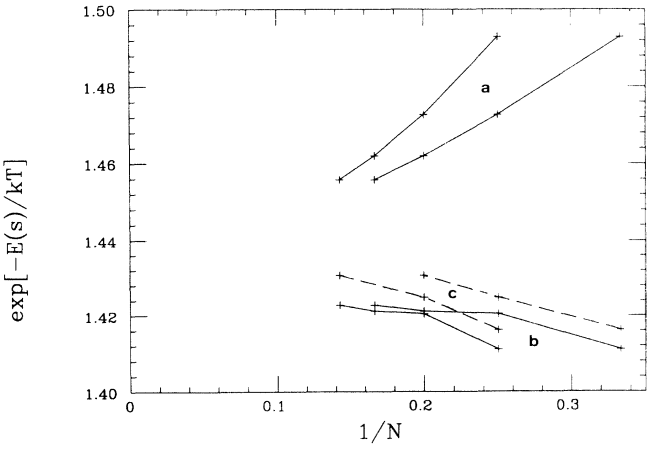

FIG. 19. The crossing points at $R = 3.0$ and $\Delta = 0.125$ of (a) the interface free energy $\eta(\pi, 0)$; (b) the interface free energy $\eta(\frac{1}{2}\pi, 1)$; and (c) the mass gap m. For each quantity two curves are shown: the crossing points as function of N and $N+1$.

At $\Delta=0.125$, the crossing points of Nm and $N\eta$'s give the same T_c within the numerical accuracy, $W=1.44\pm0.01$ (see Fig. 19). The numerical accuracy is not good enough to distinguish between a single IC melting transition (path of type 4*a*) or two transitions with a very narrow floating IC solid phase (path of type 4*b*) extending all the way to $\Delta=0$ (which implies the absence of a Lifshitz line). An analysis assuming a single transition gives results consistent with the above speculations: the temperature derivatives of ξ, of $\eta(\pi,0)$, and also of $\eta(\frac{1}{2}\pi,1)$ scale with an exponent $y_T\simeq0.95\pm0.5$; the pitch Q scales at the crossing points of m consistent with a value $x_Q=1$, but the convergence is not very convincing. I did not pursue these calculations further. The small maximum strip width is too much of a limiting factor.

VII. EXPERIMENTAL EVIDENCE

In the preceding sections we discussed the phase diagram of the four-state clock-step model; first at zero chirality, in Secs. III and IV; then at strong chirality, in Sec. V; and finally the results were combined into a global phase diagram in Sec. VI, Fig. 17. We discussed the scaling properties along the three characteristic paths through the phase diagram. Let us now compare these characteristic behaviors with the experimental results for Au(110) and Pt(110).

The deconstruction transition in Au(110) (Refs. 7, 10, and 11) is reported to have Ising-type critical exponents. The Ising exponents rule out a path of type 4*b*. The absence of a significant peak shift at the deconstruction transition disfavors a path of type 4*a*. Roughening transitions are difficult to resolve, because their thermodynamic singularities are weak, and involves a subtle change in peak shape. The characteristic power-law line shape of the rough phase must be distinguished from finite-size effects. Indications for a roughening transition in Au(110) have been reported at a temperature 50 K above the deconstruction transition.[10,11] This suggests a path of type 3. No peak shift has been reported at any temperature. This suggests a small value of $R=E_w/E_s$ or small chirality.

Robinson, Vlieg, and Kern[12] observed the onset of a shift in the MR peak in Pt(110) immediately at the deconstruction transition. The linearity of the shift $Q\sim|T-T_c|$ is consistent with a path of type 4*a* (with $x_Q=1$) and rules out a path of type 4*b* ($x_Q=\frac{1}{2}$). No direct evidence for roughening has been observed yet (i.e., a change in line shape). Roughening might take place simultaneously (path of 4*a*) or at a higher temperature (path of type 3). To explain the results in terms of a path of type 3 is difficult, however. The peak shift would be very small, except maybe when $R=E_w/E_s\simeq2$ and Δ is large. In this limit the wall excitations are composite objects, pairs of clockwise steps with opposite step height. This is the description proposed by Vilfan and Villain.[21] However, in this limit the peak shift is not likely to be linear. Vilfan and Villain presented an argument for a peak shift proportional to $Q\sim l_w/\xi^2$, which would imply $x_Q=2$. My analysis in Sec. VI (the analogy with an exactly soluble one-dimensional model) suggests a different behavior, the presence of a disorder line. The peak does not start to shift at the deconstruction transition, but only at a higher temperature (but before roughening). At disorder lines the pitch scales typically with the same (effective) exponent $x_Q=\frac{1}{2}$ as at a Pt transition (as $Q\sim|T-T_{\rm DO}|^{x_Q}$, with $T_{\rm DO}$ the disorder temperature). Neither suggestion agrees with the experimentally observed linear peak shift. Therefore, only a path of type 4*a* explains the experimental results for Pt(110).

It is not allowed to turn the argument around and to conclude that the experimental results for Pt(110) imply the existence of the Lifshitz line in Fig. 17. Suppose the Lifshitz line does not exist. Then the PT and KT transition lines (path of type 4*b*) must be very close to each other at small chirality, and experimentally this is probably not distinguishable from a true path of type 4*a*.

One of the most significant implications of the above discussion is that the chirality in Pt(110), and probably also in Au(110), must be weak. This is somewhat of a surprise. Villain and Vilfan[21] assume that chirality is strong, and also Robinson, Vlieg, and Kern[12] imply it in the analysis of their experimental data. One possible explanation might be the buckling and relaxation in the MR state, which extends to four layers deep in Au(110).[13,25] Steps and walls in the surface are probably relaxed from the sharp objects shown in Fig. 3 into more diffuse ones at a similar length scale. This does not affect their topological changes, nor the description in terms of the chiral four-state clock-step model, but might reduce the chirality considerably compared to simple estimates.

ACKNOWLEDGMENTS

I would like to thank Jacques Villain, Ed Conrad, Ian Robinson, and Glen Held for stimulating discussions on this topic. After submitting this paper for publication, I received a copy of unpublished work by Balents and Kardar where they obtain the results of Sec. V by means of the same fermion techniques. This research is supported by the National Science Foundation Grants No. DMR-88-13083 and No. DMR-9205125.

[1]K. Rommelse and M. den Nijs, Phys. Rev. Lett. **59**, 2578 (1987).

[2]M. den Nijs and K. Rommelse, Phys. Rev. B **40**, 4709 (1989).

[3]M. den Nijs, Phys. Rev. Lett. **64**, 435 (1990).

[4]M. den Nijs, in *Phase Transitions in Surface Films*, edited by H. Taub, F. G. Torzo, H. Lauter, and S. C. Fain, Jr. (Plenum, New York, 1991), p. 247.

[5]M. den Nijs, Phys. Rev. Lett. **66**, 907 (1991).

[6]G. Binnig, H. Rohrer, Ch. Gerber, and E. Weibel, Surf. Sci. **131**, L379 (1983).

[7]J. C. Campuzano, M. S. Foster, G. Jennings, R. F. Wills, and W. Unertl, Surf. Sci. **162**, 484 (1985).

[8]P. Kleban, R. Hentschke, and J. C. Campuzano, Phys. Rev. B **37**, 5738 (1988).
[9]J. Villain and I. Vilfan, Surf. Sci. **199**, L165 (1988).
[10]D. T. Keane, P. A. Bancel, J. L. Jordan-Sweet, G. A. Held, A. Mak, and R. J. Birgeneau, Surf. Sci. **250**, 8 (1991).
[11]J. Sprösser, B. Salanon, and J. Lapujoulade, Europhys. Lett. **16**, 283 (1991).
[12]I. K. Robinson, E. Vlieg, and K. Kern, Phys. Rev. Lett. **63**, 2578 (1989).
[13]E. C. Sowa, M. A. van Hove, and D. L. Adams, Surf. Sci. **199**, 174 (1988).
[14]H. S. Youn and G. B. Hess, Phys. Rev. Lett. **64**, 918 (1990); G. Hess, in *Phase Transitions in Surface Films* (Ref. 4).
[15]Y. Cao and E. Conrad, Phys. Rev. Lett. **64**, 447 (1990); P. Zeppenfeld, K. Kern, R. David, and G. Comsa, *ibid.* **62**, 63 (1989).
[16]For a review, see J. D. Weeks, in *Ordering in Strongly Fluctuating Condensed Matter Systems,* edited by T. Riste (Plenum, New York, 1980), p. 293.
[17]H. van Beijeren, Phys. Rev. Lett. **38**, 993 (1977).
[18]The step height in the BCSOS model is only half a unit cell compared to a full unit cell in the RSOS model. The lateral surface periodicity in the BCSOS model is twice as large as in the RSOS model. These two aspects negate each other.
[19]G. Mazzeo, G. Jug, A. C. Levi, and E. Toasatti, Surf. Sci. (to be published).
[20]Th. C. Halsey, J. Phys. C **18**, 2437 (1985); J. M. Thijssen and H. J. F. Knops, Phys. Rev. B **42**, 2438 (1990); E. Granato, J. M. Kosterlitz, J. Lee, and M. P. Nightingale, Phys. Rev. Lett. **66**, 1090 (1991), and unpublished results.
[21]I. Vifan and J. Villain, Surf. Sci. **257**, 368 (1991).
[22]E. H. Lieb and F. Y. Wu, Phys. Rev. Lett. **20**, 1445 (1968).
[23]V. J. Emery, A. Luther, and I. Peschel, Phys. Rev. B **13**, 1272 (1976).
[24]For a review, see M. den Nijs, in *Phase Transitions and Critical Phenomena,* edited by C. Domb and J. Lebowitz (Academic, London, 1987), Vol. 12.
[25]S. M. Foiles, Surf. Sci. **191**, L779 (1987).
[26]Hyunggyu Park and Marcel den Nijs, J. Phys. A **22**, 3663 (1989).
[27]Henk W. Blöte and Marcel P. M. den Nijs, Phys. Rev. B **37**, 1766 (1988).
[28]Marcel den Nijs, J. Phys. A **18**, L549 (1985).
[29]H. Blöte, J. L. Cardy, and M. P. Nightingale, Phys. Rev. Lett. **56**, 742 (1986); I. Affleck, *ibid.* **56**, 74 (1986).
[30]See, e.g., O. Foda, Nucl. Phys. B **300**, 611 (1988).
[31]A. B. Zamolodchikov, Pis'ma Zh. Eksp. Teor. Fiz. **43**, 565 (1986) [JETP Lett. **43**, 730 (1986)].
[32]L. P. Kadanoff and F. J. Wegner, Phys. Rev. B **4**, 3989 (1971).
[33]F. J. Wegner, Physica B **68**, 570 (1973).
[34]Marcel den Nijs, Phys. Rev. B **23**, 6111 (1981); Physica A **111**, 273 (1982).
[35]S. Tomonaga, Prog. Theor. Phys. **5**, 544 (1950).
[36]A. Luther and I. Peschel, Phys. Rev. B **9**, 2911 (1974).
[37]L. P. Kadanoff and A. C. Brown, Ann. Phys. **121**, 318 (1979).
[38]D. A. Huse and M. E. Fisher, Phys. Rev. Lett. **49**, 793 (1982).
[39]D. Tománek, H.-J. Brocksch, and K. H. Bennemann, Surf. Sci. **138**, L129 (1984).

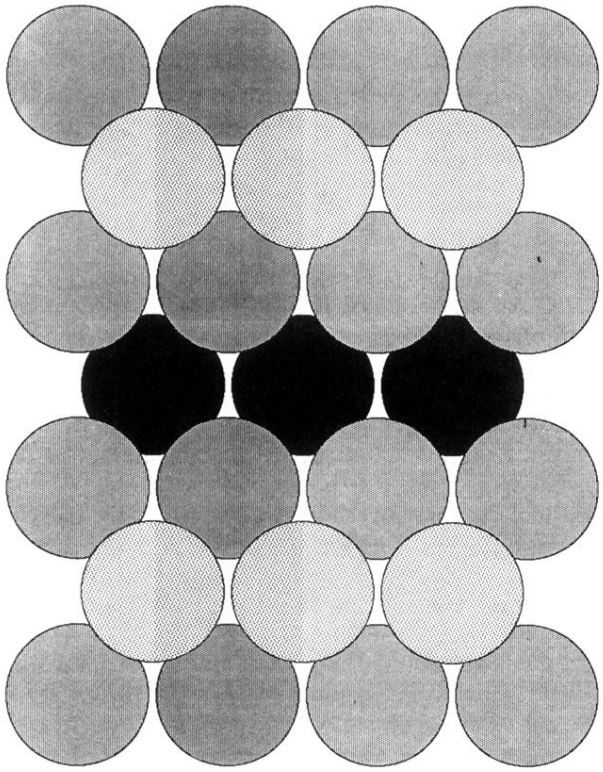

FIG. 2. Top view of a missing-row-reconstructed fcc (110) facet.